UNIVERSITY OF PADOVA

DEPARTMENT OF PHYSICS AND ASTRONOMY

Master degree in Astronomy

CORRELATION BETWEEN INSOLATION MODEL AND BOULDER DEPOSITS ON THE 67P/CHURYUMOV-GERASIMENKO COMET

Supervisor: Chiar.mo Prof. Francesco Marzari
Co-supervisor: Dott. Gabriele Cremonese

Student: PAMELA CAMBIANICA

UNIVERSITA' DEGLI STUDI DI PADOVA

DIPARTIMENTO DI FISICA E ASTRONOMIA

Corso di laurea Magistrale in Astronomia

CORRELAZIONE TRA MODELLO DI INSOLAZIONE E DEPOSITI DI BOULDERS SULLA SUPERFICIE DELLA COMETA 67P/CHURYUMOV-GERASIMENKO

Relatore: Chiar.mo Prof. Francesco Marzari
Correlatore: Dott. Gabriele Cremonese

Studente: PAMELA CAMBIANICA

Alla mia famiglia...

"L'Universo ha elargito un grande dono all'uomo:
con i suoi migliori atomi ha creato una parte di se' stesso dentro la sua mente per studiare il resto di se'.
Cosicche' le uniche leggi della materia sono quelle che la nostra mente deve architettare
e le uniche leggi della mente sono architettate per essa dalla materia."
(James Clerk Maxwell)

Abstract

Comets are considered the most fascinating and changing primordial objects of our solar system. They are not yet well understood, but they conserve important informations about the origin, the formation and the evolution of the solar system and all of its objects. From these considerations is born Rosetta, the European Space Agency mission, lanched in 2004, with the aim of study the composition, the chemical properties, the activity and the behaviour approaching the Sun during its perihelion, of 67P/Churyumov-Gerasimenko comet. The images of this short-period comet was taken in particular from OSIRIS, an Optical, Spectroscopic and Infrared Remote Imaging System onboard Rosetta. It revealed that the comet is characterized by two main lobes connected by a small neck, and that the surface is a collection of contrast, such as smooth plains or high fractured terrains. Very important features on the comet surface are the boulder deposits, i.e. positive reliefs detectable in different images with the constant presence of elongated shadows whose extension depends on the illumination geometry, and that seem to be detached from the ground where they stands. These objects are scattered all over the surface and they can be found both isolated or in cluster. In this thesis will be calculate the incidence and emission angles on some regions of the comet, the same areas studied by recent work in which it was calculated the size-frequency distribution of boulders with diameters $\geq$ 7m. In particular, the solar incidence angle will be involved to compute the total amount of absorbed solar energy for these different regions. The results show a trend between a high value of irradiation and high level of fracturing, but not for all of the regions analyzed.

Contents

Introduction

The 67P/Churyumov-Gerasimenko (hereafter 67P) is a Jupiter family comet discovered in 1969. The comet is characterized by two main lobes connected by a small neck resulting in a huge cavity and the surface is a collection of contrasts: smooth plains, scattering of boulders and imposing craggy cliffs, partially or entirely covered by dust or expose a consolidate material, pits, cliffs and fractures from the hundred meter scale to the decimeter scale. Its current orbit has an inclination $i = 7.0405°$ and an eccentricity $e = 0.64102$, a perihelion distance $q = 1.2432$ AU and a semi-major axis of 3.4630 AU resulting in a period P=6.44 years. The spin-axis orientation of cometary nucleus could be determined as RA=69° and Dec=64°, resulting in a obliquity of 52°, and the north pole is located on the bigger lobe near the neck. The volume, 21.44 km^3, and the mass, 1.0 x 10^{13} kg, of the comet yeld to a very low density of 470 kg m^{-3} and this is a clear sign of high porous interior of agglomerates.
This object is the primary target of the European Space Agency Rosetta mission: it was launched in 2004 and the spacecraft arrived at comet 67P in August 2014 entering the rendezvous phase. Rosetta is the first spacecraft to orbit a comet nucleus and, shortly after its arrival at 67P, the orbiter dispatched the Philae lander for the first touchdown on a comet nucleus. The objective mission is to study the physical and chemical properties of the nucleus, the evolution of the coma and the nucleus during the comets approach to the Sun and the development of the interaction region of the solar wind and the comet. The nucleus, its activity and the surface morphology of 67P have been observed by OSIRIS, the Optical, Spectroscopic and Infrared Remote Imaging System, on board Rosetta: it consists of a narrow- and wide-angle cameras (NAC and WAC) with a spatial scale of 18.8 cm/px when the NAC is at 10 km from the surface, while the WAC reaches a resolution of 1.01 m/px at the same distance. OSIRIS equipped with 26 medium- and narrow- band filters that cover the 240-1000 nm wavelength range.
After resolving the nucleus on June 2014 at 192 000 Km, the resolution increased reaching a scale of 18.6 cm/px duringe the 10 km orbits around 67P

and for this reason the images taken by the cameras show a detailed features on the surface. The observations point to a clear dichotomy between the two lobes, which are subjected to rather different environmental conditions. At the basis of this thesis is the ubiquitous presence on the comet surface of large blocks, called boulders, i.e. positive reliefs detectable in different images with the constant presence of elongated shadows whose extension depends on the illumination geometry, and that seem to be detached from the ground where they stands. These objects are scattered all over the surface and they can be found both isolated or in cluster, and what we want to know is how these boulders are originated.
All of these features on the cometary surface can illustrate the structure and evolution of Churyumov-Gerasimenko comet and for this reason is important to explain how some of these outlines may have arisen and what this means for our understanding of comets.
On the surface of inner planets and asteroids, boulders of various sizes have been observed by several space missions. In the large majority of the cases they seem to be related to impacts, so they are typically considered as the result of the excavation process due to a collision with a minor body. Thanks to the high resolution of OSIRIS, boulders have been observed for the first time on a cometary nucleus and, differently from inner planets and asteroids, a comet nucleus is very active and its surface is characterized by a complex thermodynamic. So it is difficult to think that impacts are the only boulder formation process on a comet, mainly considering that no evident impact crater has been recognized up to now on 67P surface. This means that other mechanisms have to be taken into account, as for example the fragmentation that in this case seems to be the most relevant one.
Fragmentation is the breaking of a continuous body into several pieces and it occurs in very distinct contexts at any scale. The aim of studying the fragmentation processes is to determine the relation among the number of initiated cracks with the density and the size of material defects, and the rate and the duration of the driving force, so to better understand the dynamic of fragmentation and the propagation of cracks. The fragments depend also on the physical regime in which they develop: in fact, in quasi-static regime the average fragment size is highly dependent on material micro- structure, providing a chaotic distribution. By contrast, in a dynamic regime, fragmentation is controlled by energy arguments, and average fragments sizes and fragment size distributions follow rather regular patterns, providing a more deterministic distribution. The limit between these two regimes is highly dependent on material and defect parameters. The application of fragmentation theory on boulder distributions as determined by the analysis of the OSIRIS images of cometary surface, would allow to understand the processes

underlying their formation and thus the evolution and structure of comet itself. The 67P surface is an active and changing environment and what is known so far about the formation and the distribution of boulders is that multiple processes expected to be at work on the surface might be related to several physical processes, like thermal stress, gravity effects and cometary activity. Getting started, the large obliquity (52°) and orientation of the 67P comet spin axis implies strong seasonal effects. The southern solstice occurs only 34 days after perihelion at a heliocentric distance of 1.24 AU and the northern solstice is reached after perihelion at 5.68 AU. This geometry leads to a thermal dichotomy: the northern hemisphere is relatively weakly illuminated for a long time, when the comet is far from the Sun; in contrast, the southern in strongly insolated during the short perihelion passages.The thermal stress occurs on the comet surface through changing insolation conditions and it is controlled by solar illumination (diurnal cycle) with the rotation period of the comet of 12,761 h, and with seasonal variation (summer and winter hemisphere). The diurnal temperature cycle is fundamental also to derive the thermo-physical properties of 67P surface: for example, temperatures as large as 230K have been measured across the nucleus surface, and this, together with the lack of detection absorption features of water ice in the spectral infrared range, indicates a porous, highly insulating surface material and a corresponding low thermal inertia. For this reasons, also considering the measured light-shadow temperature variation of the more than 50 K, it is very reasonable to assume that thermal stress can produce fractures, crack, blocks and boulders. This kind of fragmentation is related to sublimation activity of mainly water ice (but also CO_2 and CO ices, which however sublimate at a much lower temperature), a process that increases the number of small boulders and eliminates the smallest blocks containing water ice, reducing them into dust. On this respect, a recent study by Keller et al. (2015) [18] which produces a thermal and sublimation model looking at the orientation of the shape of 67P with respect to the Sun, could be extremely useful for analyzing the fragmentation process. Thanks to this model, in which the nucleus surface is simulated as a polyhedron made of ten-meter size triangular facets, it is possible to describe the diurnal insolation conditions for different areas, including the energy balance of the comet itself, due to the sunlight reflected by mutually facing facets and by their thermal IR radiation. Even the gravity gives an important contribution to the presence of boulders on comet surface: gravitational phenomena induced by differential erosion are among the most important processes on resurfacing comet 67P and this is associated with the activity of the nucleus. The erosion caused by sublimation might effect strata with different content of material and this affects scarp evolution and gravitational falls. Moreover,

the observed outburst can eject boulders and erode areas, causing new gravitational collapses; in addition, new niches and cuesta margins are formed, new accumulation deposits can be created at the basis of the walls. Some of the boulders located in these depressions can be considered as a remnant part of top layers on surface areas, so they are older and not renewed. Moreover, the activity of a comet, mainly the sudden outbursts in which a large amount of gas and dust is ejected from the comet surface in a very short time, can lift some boulders after a former fragmentation and this is the reason why they can be found isolated. Their trajectory depends on gas density or velocity, superficial gravity field, centrifugal and drag forces produced by outflowing gas. Recent studies report the larger size of liftable boulders on 67P between 2 and 6 meters. Of course, another aspect that has to be considered is a sort of secondary fragmentation, caused by subsequent impacts at the end of the lifting process.

Considering the multiple energetic processes responsible for the formation of boulders, the purpose of this thesis is to correlate the size-frequency distribution of this objects on the 67P surface with temperature maps and insolation model, in order to study the influence of the thermal energy in the formation of boulders.
Recent studies from Pajola et al.(2015) [29] give a description of the size-frequency distribution of boulders, using the Rosetta/OSIRIS cameras images of the nucleus. The spatial global size distribution corrisponds to the Northern hemisphere and covers $\sim 70\%$ of the total surface; it consists of 4976 boulders, or 3546 if are considered only objects with diameters larger than 7 m, and the slope of the power-law, with an index equal to -3.6+0.2/0.3, is different between the two lobes: the smaller one of 67P shows a more pendent global size-frequency distribution with respect to the main one and, as the two parts seem to be constituted by the some material, this is probably due to the increased erosion. A higer values of power-law means a more persuasive fracturing, i.e. a more small size boulders with respect to the larger one. The first step of this project is to analyze all images containing boulders of different size and, taking advantage of the already performed studies on the size-frequency distribution [29], all the regions where the boulders have already been cataloged. The already determined boulder global distribution shows that they are scattered everywhere on 67P surface, but that the larger of them, with diameters up to 50 meters, are located on the neck and in the Imhotep region. In particular, the cumulative boulder size-frequency distribution per km 2 of objects with diameters larger than 7 meters over the illuminated surface of the comet, can be described by power laws with different slopes for the head and the body of 67P: indeed on the head it is

much steeper than in the body, even if apparently there are not mineralogical differences between them. These different distributions need an explanation and for this reason the first step of the research will consist in analyzing the images discussed before, to characterize all regions containing boulders with their size-frequency distribution, and developing a database containing all the physical features of these objects. The basic assumption is that the boulders have to be originated by the same physical processes everywhere on the comet, and that their density is somehow related to the different fracture densities of the regions in which they are generated: thus, more fracturing would probably mean a larger number of boulders, as in the case of the head of the comet. After this classification, all studied regions must be connected with the relative comet surface temperature, because, as previously mentioned, one of the main processes responsible of the boulder fragmentation is definitely the thermal stress that the comet undergoes day by day during its orbit around the Sun. Thanks also to the data provided by VIRTIS, the Visible Infrared and Thermal Imaging Spectrometer on board Rosetta, it will be possible to create thermal maps by region and local illumination, also analyzing the temperature trend, knowing that the surface temperature depends on the physical properties of the surface, such as sublimation activity, bolometric albedo and emissivity. After that, the insolation and sublimation model, integrated along the 67P orbit, will be included to account for the different radiative energy amount that impinges on the different regions.
We expect to find smaller boulders in higher temperature regions and according to the water sublimation model, the maximum erosion is reached on the south side during the perihelion passage; in contrast the northern regions are in polar night during this phase and for the low temperature the molecules and dusty particles cannot excape from the nucleus.

Outline of the following chapters

This thesis is divided into four chapters:

In **Chapter one** is described the comets from an orbital and a physical point of view, focusing on the classifications according to their orbital parameters, and on the several part composing a comet, such as the nucleus, the coma, the tails and its activity. Moreover, in this section are listed the several cometary missions, illustrating in detail Rosetta, mission on which I focused.
The **Chapter two** deals with some important features of the comet discovered through OSIRIS, in particular the regional surface morphology, the presence of CO_2 in the comet coma, and the bond between gravitational slopes, geomorphology and material strength.
In **Chapter three** will be analyze the fragmentation process by a physical point of view and it will be connected with the size- frequency distribution of the boulders on 67P surface.
Chapter four describes our approach to the insolation and sublimation model, and to the irradiation code wich we have used to derive the value of the total insolation in regions established. These values have been connected with the boulder size-frequency distribution and this chapter shows the results of these analysis.

Chapter 1

Comet: origin, structure and exploration

A comet is an icy small Solar System body that, when passing close to the Sun, heats up and begin outgas displaying a visible coma, and sometimes also a tail: these phenomena are due to the effects of solar radiation and the solar wind upon the nucleus of the comet. Comet nuclei range from a few hundred meters to tens of kilometers across and are composed of ice, dust and small rocky particles. These objects usually have highly eccentric elliptical orbits and the range of orbital periods ranging from several years to potentially several millions of years. Short-period comets originate mainly in the Kuiper belt, whereas long-period comets are thought to originate in the Oort cloud: the Kuiper belt is a circumstellar disc in the Solar System beyond the planets, extending from the orbit of Neptune (at 30 AU) to approximately 50 AU from the Sun. It consists mainly of small bodies and most objects are composed of frozen volatiles, ices, such as methane, ammonia and water. Instead, the Oort cloud is a theoretical cloud of icy planetesimals between 50.000 AU and 200.000 AU: it is divided into two regions, a disc-shaped inner Oort cloud and a spherical outer Oort cloud. The majority of Oort objects consist of ices such water, methane, ethane, carbon monoxide and hydrogen cyanide. Comets are distinguished from asteroids by the presence of an extended, gravitationally unbound atmosphere surrounding their central nucleus. This atmosphere has parts termed the coma, the central part surrounding the nucleus, and the tail, a linear section consisting of dust or gas blown out from the coma by Sun's light pressure or outstreaming solar wind plasma.
Looking at the fate of a comet, if a comet encounters another object in the Solar System, such as Jupiter, can be ejected outside, or injected in the inner Solar System. Another scenario concerns the exhaustion of the cometary volatile, indeed most of the volatile material contained in a comet nucleus

evaporates away, and the comet becomes a small, dark, inert lump of rock or rubble that can resemble an asteroid. At least, the nucleus of some comets may be fragile and a close encounter, or thermal stress, internal gas pressure or impact, can destroy the nucleus and split the comet in several parts.

1.1 Orbital classification

Most comets are small Solar System bodies and their orbits are elongated ellipses that take them close to the Sun for a part of their orbit. Comets are classified according to the length of their orbital period, i.e. the time taken for a given comet to make one complete orbit around the Sun. The longer the period the more elongated ellipse.

1.1.1 Short period

A short-period comet (hereafter SP-comet) is defined as having orbital periods of less 200 years. The SP-comets are mostly on low-inclination prograde orbits and the arguments of perihelion ω (the angle between perihelion and ascending note) are strongly peaked near 0° and 180° [5]. It is usually believed that the SP-comets originate in the Kuiper belt. The orbits of SP-comets typically take them out to the region of the outer planets, like Jupiter, at aphelion. Comets whose aphelia are near a major planet's orbit are called its "family": SP-comets with orbital periods shorter than 20 years and low inclination, up to 30 degrees, are called *Jupiter-family comets*; those like Halley, with orbital period between 20 and 200 years, and inclination extending from zero to more than 90 degrees, are called *Halley-type comets*. Because of their elliptical orbits take them close to the giant planets, comets are subject to gravitational perturbation and for this reason their orbits are strongly influenced by the gravity of giant planets as a result of close encounters.

1.1.2 Long period

Long-period comets have orbital periods longer than 200 years and their orbits are very eccentric. By definitions they remain gravitationally bound to the Sun and these comets are ejected from the Solar System due to close passes by major planets and they are non longer considered as having a period. The orbit of long-period comets take them far beyond the outer planets at aphelia, and the plain of their orbits need not lie near the ecliptic. These object also have parabolic or slightly hyperbolic trajectories when near perihelion in the inner Solar System. They originate in the spherical shell of

icy bodies known as the Oort Cloud, and they may be perturbed from their resting place in the Oort cloud by a passing star or giant molecular cloud, or even through tidal forces generated by the bulge and disk of our Galaxy. Such gravitational influences may send these icy bodies on a path towards the centre of the Solar System in highly elliptical orbits. Originating from a spherical distribution, the high inclinations of the orbits arise since they can enter the inner Solar System from any angle. A long period comet is called *new* if its major semi-major axis is greater than 10000 AU, *returning* if it is less than 10000 AU.
Long-period comets tend to be the most spectacular comets we see in the night sky: their brilliance is due to the fact that they have not made many (if any) passes through the inner Solar System, and so still retain a large percentage of their volatiles.

1.2 Physical characteristics

1.2.1 Nucleus

The nucleus is the solid, central part of a comet, composed of rock, dust, and frozen gases. When heated by the Sun, the gases sublimate and produce an atmosphere surrounding the nucleus known as the *coma*. The force exerted on the coma by the Sun's radiation pressure and solar wind cause an enormous *tail* to form, which points away from the Sun.
The chemical composition of a comet nucleus has often been described as a dirty snow ball, but it is commonly assumed that comet nuclei have an atomic composition which is well represented by Solar System abundances of condensable elements. If one accepts the two basis premises that comets are homogeneus aggregates of core-mantle interstellar dust grains and that the comets contain the Solar System abundances of the condensable elements, the inhevitable consequence is that abou 30% of the mass of a comet nucleus is H_2O [12]. Other elements that are found in the nucleus are frozen carbon monoxide (CO), carbon dioxide (CO_2), methane (CH_4) and ammonia (NH_3).
A typical comet nucleus has an albedo of 0.04: it is extremely dark black due to a crust of dust and rock that covers most of the ice. These comets release gas only when holes in this crust rotate toward the Sun, exposing the interior ice to the warming sunlight.
Rougly six percent of the Near Earto Asteroids are thought to be extinct nuclei of comets, which no longer experience outgassing, because they have expelled most of their volatile ice.

1.2.2 Coma

The coma is the nebulous envelope around the nucleus of a comet and if the comet nucleus is pulled into an orbit which carries it close to the Sun, the solar heat will cause the outer layers of the icy nucleus to evaporate. During this process, dust and gases which form the coma around the nucleus are released and as the comet gets closer to the Sun, the coma grows. The solar wind push the dust and gas away from the coma causing them to stream off into space to form the comet's tail. The coma is generally made of ice and comet dust, and water dominates up to 90% of the volatiles that outflow from the nucleus when the comet is within 3-4 AU from the Sun. The shape of the coma can vary for the same comet during its apparition, depending on the comet's distance from the Sun and the relative amount of dust and gas production. While for faint comets or bright comets producing little dust, the coma is usually round, comets which are producing significant quantities of dust have fan-shaped or parabolic comae. This is due to the different size of the dust grains released: the larger get left along the comet's orbital path while the smaller can be pushed away from the Sun by light pressure.

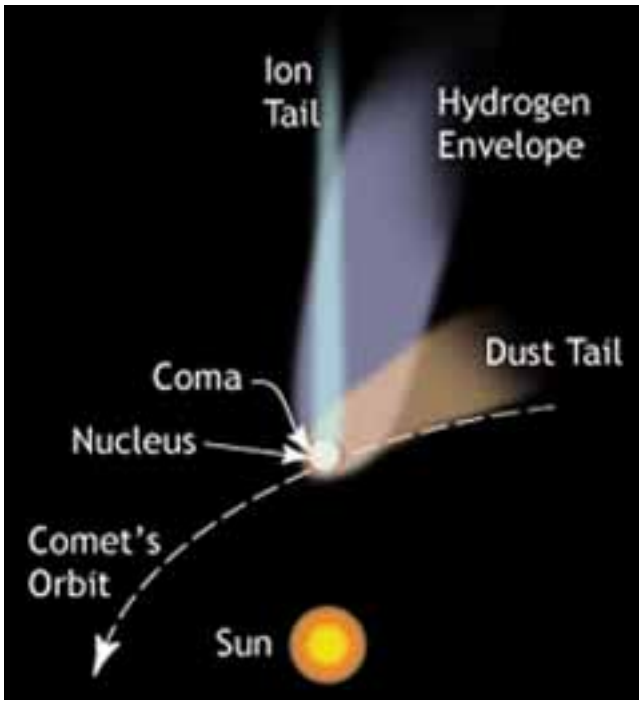

Figure 1.1: Section of a comet

The coma has two main constituents: the gas coma and the dust coma. The gas coma consists of molecules liberated from the nucleus by solar heat-

ing and relative sublimation. Once they have left the nucleus, these molecules in the coma are exposed to direct solar radiation and can be damaged in various ways: due to the combined action of these reactions, most molecules are dissociated within a day of their leaving the nucleus. The most usual among these reactions is photo-dissociation: the molecule (called "parent molecule") absorbs a photon form the Sun's radiation and breaks into two pieces (called "daughter molecules"). These daughter molecules are quite easy to observe because they have strong spectral lines at optical wavelengths. In addition to being photo-dissociated, gas species in comets can also be ionized. The formed ions are susceptible to a magnetic force due to the solar magnetic field carried by the solar wind. Consequently, the ions are swept almost radially away from the Sun, into a long, distinctive tail, called the ion tail. The outflow speed of the coma combined with the lifetime of molecules, determine the dimension-scale of the coma. In one day, at 1 Km/s, molecules can travel about 50,000 Km and this is the approximate radius of the gas coma. Instead, the dust grains that form the dust coma are dragged from the nucleus by the rush of sublimating gas. The speed of these grains will be accelerated to, depends mostly on their size, since smaller grains are lighter and therefore much more accelerated by the gas. The grains can become part of the coma only if they reach a speed greater than the nucleus escape velocity. Grains that are too large to be ejected, fall back to the surface and may become part of a the nucleus mantle. The lighter grains, instead, leave the nucleus and are in free flight around the Sun, since the nuclear gravity of the comet is very weak. Cometary dust grains are found of all sizes: the grains that are most visible to the eye have diameters of about 0.001 mm but even grains of many tens of centimeters can be ejected by the gas flow from a very active, near-Sun comet. Many of these grains pass from the tail into the interplanetary medium.
Each time the comet passes close to the Sun, it loses some of its material. Over time, it will break up and disappear completely.

1.2.3 Tails

As a comet approaches the inner Solar System, solar radiation causes the volatile materials within the comet to vaporize and stream out of the nucleus, carrying dust away with them. The force exerted out to coma by the Sun's radiation pressure and solar wind cause a tail to form, which points away from the Sun, as shown in the figure 1.2.

The streams of dust and gas each form their own distinct tail, pointing in slightly different directions.
The tail of dust is left behind in the comet's orbit in such a manner that

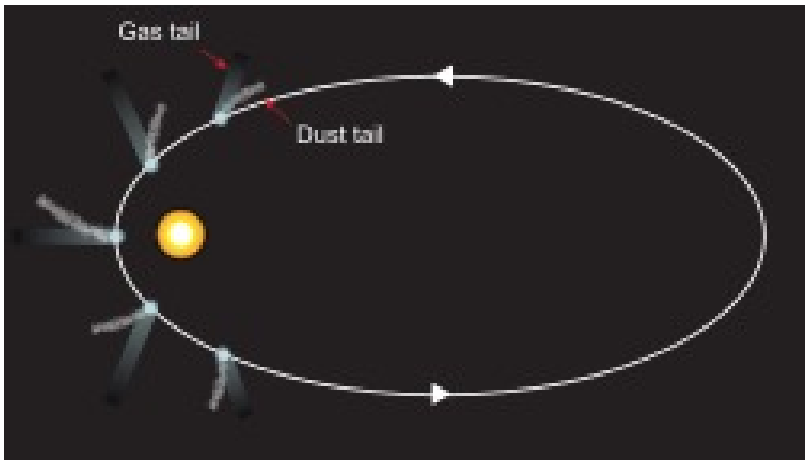

Figure 1.2: The different directions of the gas and dust tails as the comet passes the Sun

it often forms a curved tail called the antitail, only when it seems that it is directed towards the Sun. At the same time, the ion tail, made of gases, always points along the streamlines of the solar wind as it is strongly affected by the magnetic field of the plasma of the solar wind. The ion tail is the result of ultraviolet radiation ejecting electrons off particles in the coma. Once the particles have been ionised, they form a plasma which in turn induces a magnetosphere around the comet. The comet and its induced magnetic field form an obstacle to outward flowing solar wind particles. The comet is supersonic relative to the solar wind, so a bow shock is formed upstream of the comet (i.e. facing the Sun), in the flow direction of the solar wind. In this bow shock, large concentrations of cometary ions (called "pick-up ions") congregate and act to "load" the solar magnetic field with plasma. The field lines drape around the comet forming the ion tail. If the ion tail loading is sufficient, then the magnetic field lines are squeezed together to the point where, at some distance along the ion tail, magnetic reconnection occurs. This leads to a tail disconnection event. Parallax viewing from the Earth may sometimes mean the tails appear to point in opposite directions.

1.2.4 Activity

Uneven heating can cause newly generated gases to break out of a weak spot on the surface of comet's nucleus, like a geyser. The observed jets can be produced by acceleration of evolved gas from a subsurface cavity through a narrow hole to the surface. As long as the cavity is larger than the hole, the pressure in the cavity will be greater than the ambient pressure in the

coma and the flow from the geyser will be supersonic. The gas flow becomes collimated as the sound speed is approached and dust entrainment in the gas flow creates the observed jets. Outside the cavity, the expanding gas loses its collimated character, but the density drops rapidly decoupling the dust and gas, allowing the dust to continue in a collimated beam. These streams of gas and dust can cause the nucleus to spin, and even split apart.

1.3 The importance of a cometary mission

The formation environment of comets in the primordial nebulae is related to the sublimation sequence for various species of possible constituents of the nuclear ice, which would have condensed on the grain surface. The most important reason to study a comet is its origin and composition, because it reflects the primordial components of the Solar System.
Furthermore, there are a lot of theories about the correlation between comets bombardment and life on Earth: many comets and asteroids collided into Earth in its early stages and about 4 billions years ago comets bombarding our planet carrying the vast quantities of water that now fill the Earth's oceans. In addition, the detection of organic molecules, including polycyclic aromatic hydrocarbons, on the cometary surface, led to believe that these objects are the precursors of life on Earth: comets are known to harbour simple ices and the organic precursors of the building blocks of proteins, amino acids, that are essential to life. Impacts of icy bodies, such as comets, onto rocky surfaces, and, equally, impacts of rocky bodies onto icy surfaces, could have been responsible for the manufacture of these complex organic molecules through a process of shock synthesis; indeed the hypervelocity impact shock of a typical comet ice mixture produced several amino acids after hydrolysis [24].

1.3.1 Space missions

The main spacecraft mission about a comet and its activity are:

- **Giotto**: the first really close mission to a comet nucleus was space probe Giotto. This was the first time a nucleus was imaged at such proximity, coming as near as 596 km. The data was a revelation, showing for the first time the jets, the low-albedo surface, and organic compounds;

- **International Cometary Explorer**: launched on 1978 to study the interaction between the terrestrial magnetic field and the solar wind,

in 1982 the mission changed and it studied the influence of the solar wind on a cometary surface;

- **Deep Impact**: the aim of the mission is study how much ice is in a comet. In 2001, the Deep Space 1 spacecraft obtained high-resolution images of the surface of comer Borrelly: it was found that this surface is hot and dry, and extremely dark, suggesting that the ice has been removed by solar heating. In July 2005, the Deep Impact studied the interior of a comet crater on Temple 1;

- **Stardust**: the mission studied the materials retrieved from the tail of Wild 2 comet. This object contains crystalline grains that formed in the hot inner Sola System.

1.4 Rosetta mission

Rosetta is a planetary cornerstone mission in European Space Agency's Horizon 2020 long-term program and it was launched on 2 March 2004 to comet 67P/Churyumov-Gerasimenko, a short period comet of the Jupiter family. Originally, Rosetta was targeted to another Jupiter family comet, 46P/Wirtanen, with launch in January 2003. However the launch had to be delayed owing to unforeseen problems with the launch vehicle and 67P/ Churyumov-Gerasimenko (hereafter 67P) was identified as the new target comet. The objective mission is to study, with a combination of remote sensing and situ measurements, the physical and chemical properties of the nucleus, the evolution of the coma and the nucleus during the comet's approach to the Sun and the development of the interaction region of the solar wind and the comet. The spacecraft consists of the Rosetta orbiter, which features 12 instruments, and the Philae lander, with nine additional instruments.
During the cruise phase, Rosetta has observed the asteroid 2867 *Steins*, in September 2008, and the asteroid 21 *Lutetia*, in July 2010. Rosetta reached comet 67P on 6 August 2014 following a 10-year journey through the Solar System. Between August and November 2014, the spacecraft orbited the comet and gathered data to characterise the nucleus and its environment. Rosetta is the first spacecraft to orbit a comet nucleus and, shortly after its arrival at 67P, on 12 November 2014 the orbiter dispatched the *Philae* lander for the first touchdown on a comet nucleus. The orbiter tracked the comet through perihelion (August 2015), examining its behaviour before, during and after this event. The nominal end of the mission was scheduled

for December 2015, but Rosetta mission has been extended until September 2016.

1.4.1 History of the mission

The records of the Rosetta mission start on its way to comet 67P, in fact Rosetta passed through the main asteroid belt and made the first European close encounter with several of these primitive objects. Moreover, Rosetta is the first spacecraft to orbit a comet nucleus and to fly alongside a comet as it heads towards the inner Solar System and, finally, shortly after its arrival at 67P, the Philae lander made the first controlled touchdown on a comet nucleus, and it obtained the first images from the comet's surface and made the first in-situ analysis of its composition.
Rosetta was set to be launched on 12 January 2003 to rendezvous with the comet 46P/Wirtanen in 2011; this plan was abandoned because unforseen problems with the launch vehicle. For this reason, the comet 67P/Churyumov-Gerasimenko became the primary target of the mission and the revise launch date was postponed to 26 February 2004. After two launch attempts, Rosetta was launched on 2 March 2004 at 7:17 GMT from the Guiana Space Center in French Guiana.
Once in orbit, to achieve the required velocity to rendezvous with 67P, Rosetta used gravity assist manoeuvres to accelerate throughout the inner Solar System. A gravitational slingshot is the use of the relative movement and gravity of a planet or other object to alter the path and the velocity of a spacecraft, in order to save propellent, time and expense.
The first Earth flyby was on 4 March 2005 and on February 2007, the spacecraft was scheduled for a low-latitude flyby of Mars, in order to correct the trajectory.
The second Earth flyby was on 13 november 2007 at a distance of 5700 kilometers. The spacecraft performed a close flyby of asteroid 2867 Steins on 5 September 2008 and on July 2010, Rosetta flew by 21 Lutetia, a large main-belt asteroid. The third and final flyby on earth happened on 12 November 2009. In August 2014, Rosetta encountered the comet 67P and commenced a series of manoeuvres that took it on two successive triangular path, averaging 100 and 50 kilometers from the nucleus. After closing to within about 30 kilometers from the comet on 10 September, the spacecraft entered actual orbit about it.
Philae detached from Rosetta on 12 November 2014 at 8:35 UTC, and approached 67P at relative speed of about 1 km/s. This velocity is the same comet's escape velocity and for this reason, on contact with the surface, the lander has been anchored to prevent it from bouncing off. The released and

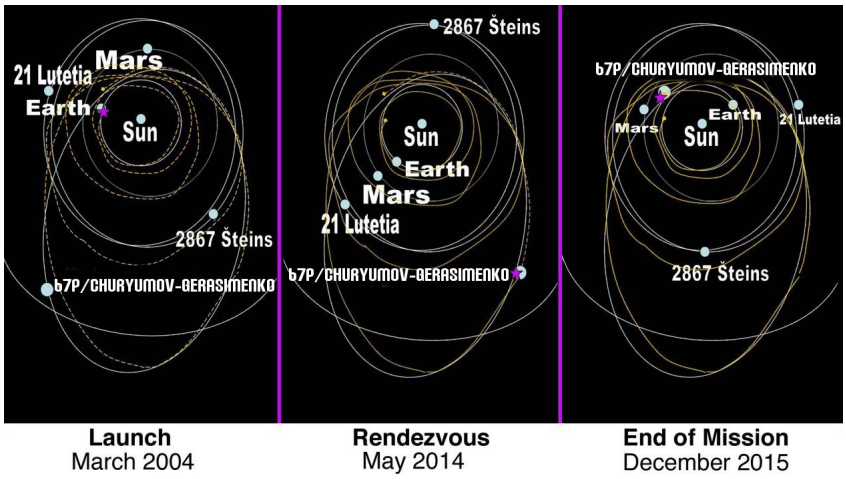

Figure 1.3: Trajectory of the Rosetta spacecraft

descendent happened as planned, precisely documented by imaging, ranging, thermal mapping, and the evolution of the magnetic properties. Primary analysis indicated that surface is relatively soft, covered with a layer of granular material about 0.25 meters deep. The role of Philae includes the characterisation of the nucleus, determination of chemical compounds, and study of comet activities and developments over the time. Unfortunately, it landed likely in the shadow of a nearby cliff or crater wall and canted at an angle of around 30 degrees. This made it to unable to adequately collect solar power, and it lost contact with Rosetta when its batteries run out after two days. Contact was briefly and intermittently restablished several months later between 13 June and 9 July, before contact was lost once again. Rosetta and Philae have been in hibernation until January 20, 2014. After the successful wake up, they underwent a post hibernation commissioning.

1.4.2 Instruments

Remote sensing instruments

The investigation of the nucleus is done by three optical spectrometers, one microwave radio antenna and one radar:

- ALICE-Ultraviolet imaging spectrograph.
  It is a lightweight and low-power spectrograaph optimized for cometary far-ultraviolet spectroscopy. It is designed to obtain spatially-resolved spectra of 67P targets in the 700-2050 Å spectral band, with a spectral resolution between 8 Å and 12 Å. During cruise the comet, ALICE

will make observations of Steins and Lutetia, of Mars and its moons, and of Earth's moon. The Ultraviolet spectrograph will search for and quantify the noble gas content in the comet nucleus;

- VIRTIS-Visible and Infrared Thermal Imaging Spectrometer.
  The Visible and IR spectrometer is able to detect and characterise the evolution of specific signatures such as the typical spectra band of minerals and molecules arising from surface components and from material dispersed in the coma. Moreover, the surface thermal evolution during comet approach to Sun will be also studied. The first observatios of VIRTIS was the vibrational bands of H_2O and CO_2 at 2.67 and 4.27 μm from 24 November 2014 to 24 January 2015, looking that the water production of 67P did not increase much from 2.9 to 2.5 AU;

- MIRO-Microwave Instrument for the Rosetta Orbiter.
  The abundance and temperature of volatile substances like water, ammonia and carbon dioxide can be detected by this instrument via their microwave emissions. It consists of a 30-cm diameter, offset parabolic reflector telescope followed by two heterodyne receivers. The submillimeter radiometer/spectrometer is fixed tuned to measure four volatile species CO, CH_3OH, NH_3 and three, oxygen-related isotopologues of water, $H_2^{16}O$, $H_2^{17}O$ and $H_2^{18}O$. The basic quantities measured with the MIRO instrument are surface temperature, gas production rates and relative abundances, and velocity and excitation temperature of each species, along with their spatial and temporal variability;

- CONSERT-Comet Nucleus Sounding Experiment by Radiowave Transmission.
  This experiment will provide information about the deep interior of the comet using a radar. The radar will perform tomography of the nucleus by measuring electromagnetic wave propagation between the Philae lander and the Rosetta orbiter through the comet nucleus. This allows it to determine the comet's internal structure and deduce information on its composition;

- RSI-Radio Science Investigation.
  This instrument makes use of the probe's communication system for physical investigation of the nucleus and the inner coma of the comet.

OSIRIS

OSIRIS-Optical, Spectroscopic and Infrared Remote Imaging System. This instrument comprises a high resolution Narrow Angle Camera (NAC) unit and a Wide Angle Camera (WAC) unit: the NAC is designed to obtained high resolution images of the surface of comet 67P through 12 discrete filters over the wavelength range 260-1000 nm at an angular resolution on 18.6 μrad/px. The WAC is optimized to provide images of the near-nucleus environment in 14 discrete filters at an angular resolution of 101 μrad/px. The OSIRIS has to observed the nucleus, its activity and surrounding down to a scale of $\sim$ 2 cm/px;

In situ instruments

The scientific objects of these instruments are to study the composition of gas and dust particles, and the solar wind interaction:

- ROSINA-Rosetta Orbiter Spectrometer for Ion and Neutral Analysis. This spectrometer consists of two mass spectrometers for neutrals and primary ions with complementary capabilities and a pressure sensor. To ensure that absolute gas densities can be determined, each mass spectrometer carries a reservoir of a calibrated gas mixture allowing in-flight calibration. Furthermore, identical flight-spares of all three sensors will serve for detailed analysis of all relevant parameters, in particular the sensitivities for complex organic molecules and their fragmentation patterns in our electron bombardment ion sources;

- MIDAS-Micro-Imaging Dust Analysis System.
  This system will provide 3D images and statistical parameters of pristine cometary particles in the nm-μm range from comet 67P. According to cometary dust models and experience gained from the Giotto and Vega missions to 1P/Halley, there appears to be an abundance of particles in this size range, which also covers the building blocks of pristine interplanetary dust particles. The dust collector of MIDAS will point at the comet and collect particles drifting outwards from the nucleus surface. MIDAS is based on an Atomic Force Microscope (AFM), a type of scanning microprobe able to image small structures in 3D. AFM images provide morphological and statistical information on the dust population, including texture, shape, size and flux;

- COSIMA-Cometary Secondary Ion Mass Analyser.

This instument is based on the analytic measurement method of secondary ion mass spectrometry (SIMS). The experiments goal is in-situ analysis of the elemental composition (and isotopic composition of key elements) of cometary grains. The chemical characterization will include the main organic components, present homologous and functional groups, as well as the mineralogical and petrographical classification of the inorganic phases;

- GIADA-Grain Impact Analyser and Dust Accumulator.

  It is devoted to study the cometary dust environment; GIADA will be plunged in the dust environment of the coma and will be able to explore dust flux evolution and grain dynamic properties with position and time;

- RPC-Rosetta Plasma Consortium.

  The Rosetta Plasma Consortium will make in-situ measurements of the plasma environment of comet 67P. The consortium will provide the complementary data sets necessary through five sensors for an understanding of the plasma processes in the inner coma, and the s tructure and evolution of the coma with the increasing cometary activity.

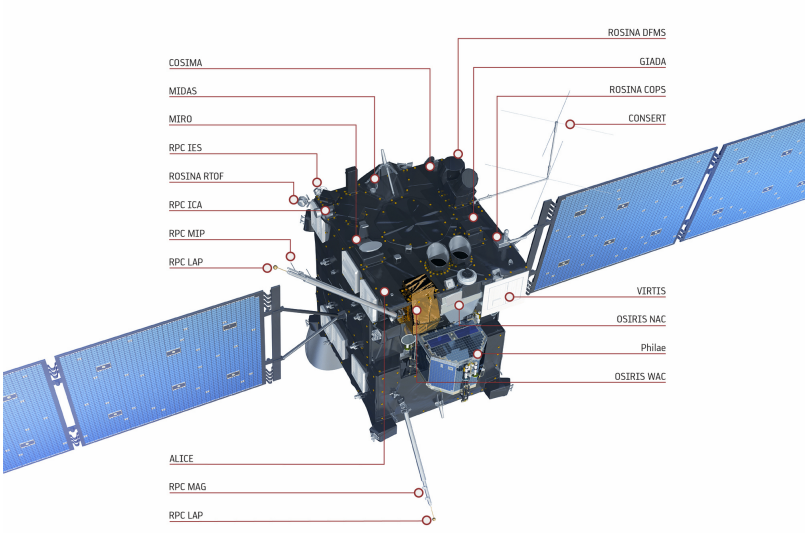

Figure 1.4: Pyload instruments onboard Rosetta spacecraft

Philae

Philae is a robotic European Space Agency lander that accompained the Rosetta spacecraft. The science payload of the lander consists of ten instruments:

- APXS-Alpha Particle X-ray Spectrometer.
  This spectrometer detects alpha particles and X-rays, which provide information on the elemental composition of the comet's surface;
- CIVA-Comet nucleus Infrared and Visible Analyser.
  A group of seven identical cameras used to take panoramic pictures of the surface plus a visible-light microscope and an infrared spectrometer. The panoramic cameras (CIVA-P) are arranged on the sides of the lander at 60° intervals: five mono imagers and two others making up a stereo imager. Each camera has a 1024x1024 pixel CCD detector. The microscope and spectrometer (CIVA-M) are mounted on the base of the lander, and are used to analyse the composition, texture and albedo of samples collected from the surface;
- CONSERT-COmet Nucelus Sounding Experiment by Radiowave Transmission.
  This instruments will use electromagnetic wave propagation to determine the comet's internal structure;
- COSAC-COmetary SAmpling and Composition.
  This instrument is a combined gas chromatograph and time-of-flight mass spectrometer to perform analysis of soil samples and determine the content of volatile components;
- MUPUS-MUlti-PUrpose Sensor for Surface and Sub-Surface Science.
  This sensor measure the density, thermal and mechanical properties of the comet's surface;
- Ptolemy
  An instrument measuring stable isotope ratios of key volatiles on the comet's nucleus;
- ROLIS-ROsetta Lander Imaging System.
  The CCD camera used to obtain high-resolution images during descent and stereo panoramic images of areas sampled by other instruments;
- ROMAD-Rosetta Lander Magnetometer and Plasma Monitor.
  Magnetometer and plasma sensor to study the nucleus' magnetic field and its interactions with the solar wind;

- SD2-Sampling, Drilling and Distribution.
  System obtains soil samples from the comet and transfers them to the Ptolemy, COSAC, and CIVA instruments for in-situ analysis;

- SESAME-Surface Electric Sounding and Acoustic Monitoring Experiments.
  Three instruments to measure properties of the comet's outer layers. The Cometary Acoustic Sounding Surface Experiment (CASSE) measures the way in which sound travels through the surface. The Permittivity Probe (PP) investigates its electrical characteristics, and the Dust Impact Monitor (DIM) measures dust falling back to the surface.

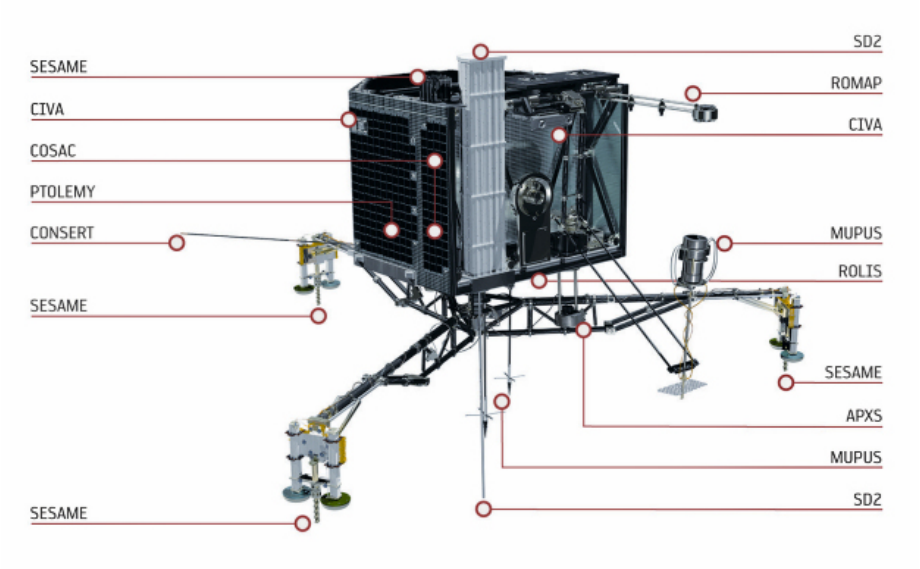

Figure 1.5: Payload instruments onboard Philae lander

Chapter 2

Comet 67P/Churyumov-Gerasimenko

In 2003, comet 67P/Churyumov-Gerasimenko (hereafter 67P) was selected as a new target of the Rosetta mission as the most suitable alternative to the original target, 46P/Wirtanen. It was discovered in 1969 and it belongs to the Jupiter-family: this kind of comet has a short orbital period, and in the case of 67P the orbital period is less than 20 years, and the name comes from the gravitational influence of Jupiter. In particular 67P comet has a perihelion distance of 1.29 AU and a period of 6.57 years. Images of comet 67P acquired by OSIRIS (Optical, Spectroscopic and Infrared Remote Imaging System) imaging system on board Rosetta show a wide variety of different structures and textures. In particular the images reveal that 67P is characterized by two main lobes connected by a region called the *neck* located between them, and the surface is a collection of contrasts: in fact, there are a lot of smooth plains, scattering of boulder, imposing craggy cliffs, pits, fractures, from hundred meter scale to decimeter scale, partially or entirely covered by dust or expose a consolidated material. The upper lobe of 67P is fairly homogeneous on a spatial scale of tens of meters. The average permittivity provides ranges of the volumetric dust/ice ratio and the internal porosity. The dust component may be comparable, from the dielectric properties, to that of carbonaceous chondritic meteorites. COSAC and Ptolemy independently measured the composition of the volatile constituents of the grains lifted at touchdown and of the species outgassed at the final landing site. The grains are primarily made of carbon-rich species in a complex suite of molecules, including precursors to some biomolecules and other compounds never before identified in comets.
The comet shape raises the question of whether two lobes represent a contact binary formed 4.5 billion years ago, or a single body where a gap has evolved

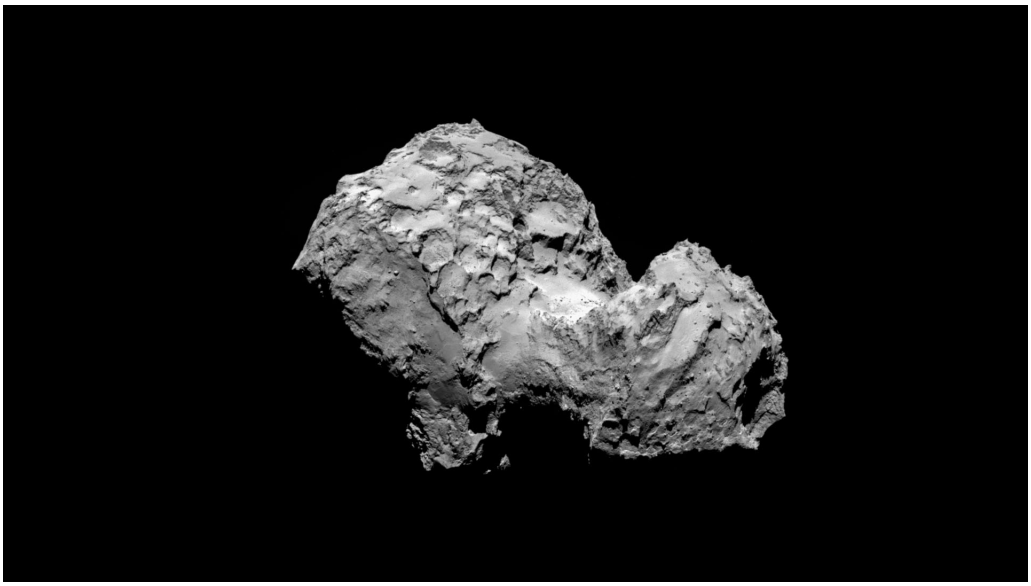

Figure 2.1: Comet 67P/Churyumov-Gerasimenko

via mass loss. The surface morphology suggest that the removal of large volume of material, mainly via sublimation or explosive release of surface pressure, may be a major mass loss process. The nucleus has a density of 535 kg/m^{-3} [32], less than half that of water, and the activity is predominantly from the neck, where jets have been seen consistently.
67P is non-magnetized on a scale of less than a meter, with its surface layers composed of both sintered ices, which are hard in nature, and fluffy grains and pebbles of organic materials, possible remnants from the era of comet formation itself.
Taken together, these first measurements performed at the surface of 67P profoundly modify the vision of comets had until now.

2.1 Constraints on 67P origin from OSIRIS observations

The importance of the Rosetta mission lies in the possibility to investigate the origin of the Solar System by exploring comet 67P at close range. First of all, the exact place in which the comet has formed is very difficult to say, but some regions, as the areas inside the orbit of giant planets, can be descarded because ices condensed at cooler zones. Currently, the tran-planetary space is favored as the birth place of comet nuclei.

Thanks to the OSIRIS images of the 67P nucleus, it can be possible to regard the origin and the evolution of the comet itself. As shown by the OSIRIS images, the 67P comet is characterized by two lobes: looking at the current shape, spin axis orientation and homogeneus composition, 67P comet is a candidate to be a contact binary. The comet shape is very unusual, since the two lobes have their longest axes nearly perpendicular and not aligned. Some morphological features support the hypothesis of a bi-lobate nature of 67P due to collision and merging of two distinct objects: in fact the high porosity of 67P and the content of volatile species are factors in support of this thesis. There are two possible formation scenarios of the comet 67P: the first is that the comet is the result of a low-speed and inelastic collision between two planetesimals and this happened in the earlier stages of the disk evolution. The second hypothesis is that 67P is the result of re-accumulation of fragments created during a catastrophic collision. Numerical simulations have shown that the two lobes are two distinct objects that merged in a low-speed collision, but it is not clear if the parts are primordial planetesimals or they are fragments produced by a collision. The origins of internal layers remain elusive and according to Groussin at al. (2015) [13], the low compressional strength of the comet may stimulate pressure that induced layering.

2.1.1 Regional surface morphology of 67P

The OSIRIS images reveal that the comet 67P is characterized by two main lobes connected by a small region, called "neck". Looking at the shape model of the comet, the larger lobe (hereafter the body) has a size of 4.1x3.3x1.8 km, whereas the head, i.e. the smaller lobe, is 2.6x2.3x1.8 km [34].

There are 19 regions on the currently illuminated surface of comet 67P and the nucleus shows a morphological diversity classified into consolidate regions, non-consolidated regions, with smooth terrains and dust-covered regions, and large irregular depression. The consolidate region is the most common region type and it discloses several fractures; for this reason, the body displays very low bulk density.
Following, can be found a basic description and morphology of the various regions described in El-Maarry et al. (2015) article [6]:

- **Body**
  - *Khepry*: strongly consolidated, rough- and bright-looking unit neighboring the Imhotep, Aten, Babi, and Aker regions. Moderately lineated. Rough in comparison to Aker although transition to it is gradual. Numerous ponds of smooth deposits.

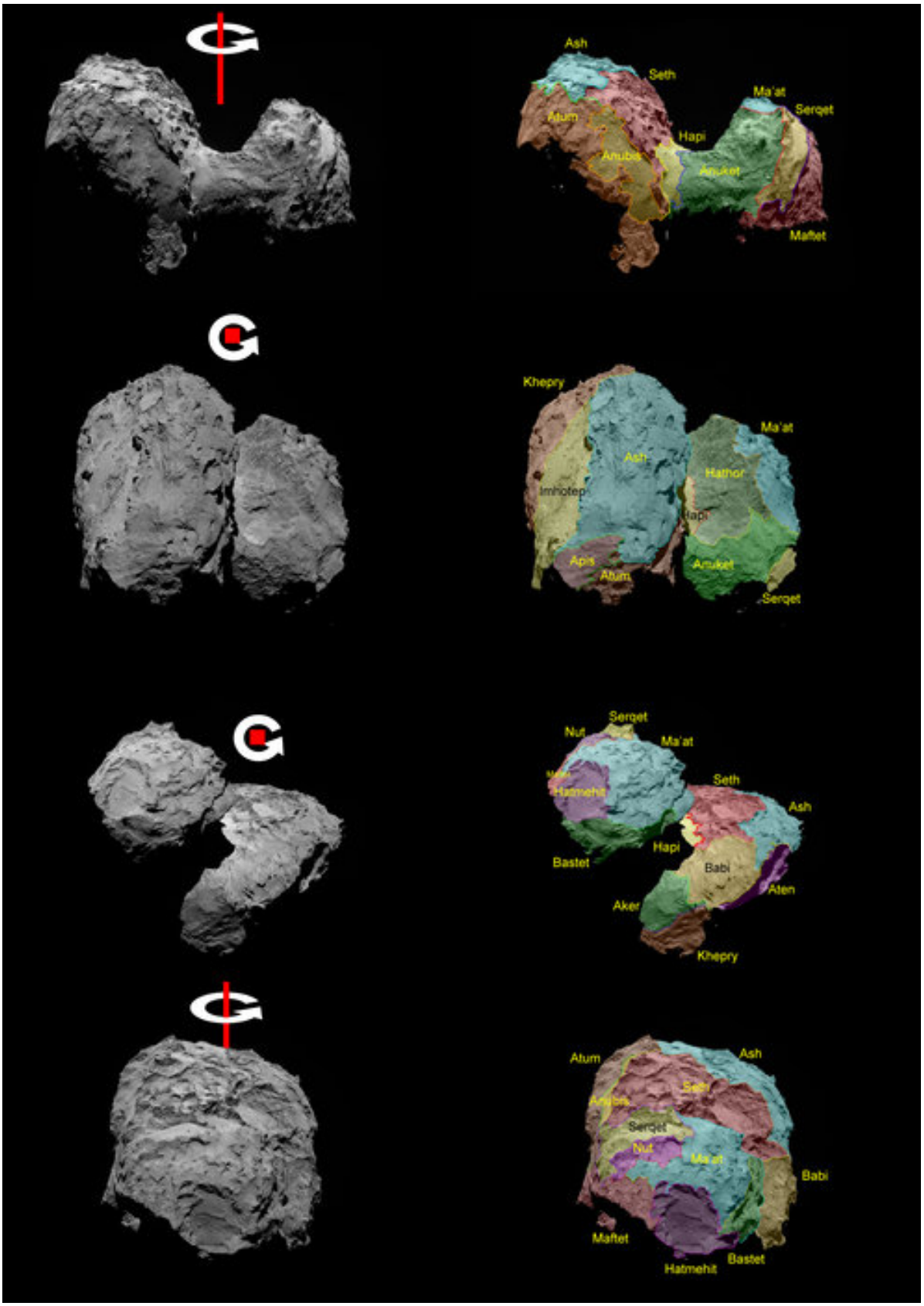

Figure 2.2: *left*: WAC and NAC images showing the comet in different orientations. *right*: same images with regional boundaries and nomenclature superposed.

- *Aker*: strongly consolidated, dark-toned unit with a mixed degree of roughness. Lineated and showing tectonic-like features. Possibly a reworked section of the Khepry region. Several small smooth areas are evident. 200 m-long angular fractures.
- *Imhotep*: non-consolidate, smooth material. Geologically the most diverse region on 67P. Extremly smooth, probably recently resurfaced, yet bouldered region enclosed by horizontally bedded and vertically jointed ridges. There is strong evidence of mass-wasting all around the smooth areas well as the presence of conical structures and pits that are possibly the result of mechanisms similar to mud volcanism. In this region there is a field of large boulders.
- *Ash*: non-consolidate and dust-covered material. Main debris-covered region of the body. Very fine deposits possibly a few meters thick. Similar to Ma'at region. Contains the only currently identified candidate impact crater on the surface of the comet.
- *Seth*: generally lacking a dust cover, yet bouldered region with ubiquitous circular, semi-circular, and quasi-circular features that display polygonal cracks in some places. Strong evidence of collapse. Possibly underlies the dust in Ash. Sharp topographic contact with Anubis.
- *Aten*: well-defined depression between the Imhotep, Ash, Babi and Khepry regions. Not covered by debris from Ash. Possibly formed through a violent short-term event. High concentration of talus deposits and rockfalls.
- *Babi*: transitional region that grades smoothly into Ash and Seth regions in terms of dust cover. Neighbors the Aten, Khepry and Aker regions as well and displays exposures of brittle mantling material at its contact with the Aten depression.
- *Apis*: strongly consolidated, flat, smooth and lineated unit showing irregular and polygonal lineations. Significant topographic change with respect to Atum and Imhotep. Polygonal crack patterns.
- *Atum*: strongly consolidated and highly complex region. Minimal bouldering but severall small depressions showing some lineation. Irregular complex mounds also seen. Borders the Anubis unit with ill-defined margins in places.
- *Anubis*: non-consolidated and smooth region very similar to Imhotep and, possibly, Hapi. Some scattered boulders possibly a result of

mass-wasting. Smooth deposits appear faulted/folded in some regions and display linear features similar to those observed in Imhotep.

- **Neck**
  - *Hapi*: non-consolidated and smooth region connecting the head and body of comet. Currently the most active region and site of regular jet activity although exact source not defined. Smooth dusty-looking material along with dispersed large boulders that may have slumped from the head or body regions. Linear field of large boulders.
- **Head**
  - *Hator*: strongly consolidated region, a 900 m-high cliff that is opposite to the Seth region on the body and rising above the Hapi region. Un-mantled and heavly lineated in two dimensions. Shows signs of detachment. Lighting makes the lineated appearance appear very uniform but other viewing angles show that it is rough.
  - *Anuket*: strongly consolidated and complex unit, that is separated from Hathor by a scarp. Parallel lineations evident on Hator are absent. It is separated from Ma'at and Maftet. Peculiar "melted wax"-like overall morphology.
  - *Ma'at*: non-consolidated and dust-covered region, the most covered on the head. Similar to Ash. Smooth deposits showing ripple-like structures, a possibly sign of mobilization. Sharp outcrops of underlying material are usually observed.
  - *Serqet*: small strongly consolidated material region encompassing a sharp ridge and a flat and smooth plain with few boulders.
  - *Nut*: small depression between the Serqet ridge and the Ma'at /Hatmehit region. Heavly bouldered and possible result of erosion of Serqet.
  - *Maftet*: strongly consolidated and rough terrain, lineated, and bouldered with scattered patches of debris neighbooring the Hatmehit, Nut and Serqet regions. Many small irregular depressions and pits which give the appearance of lifted blocks/chunks of material and possible fluidized activity.
  - *Bastet*: strongly consolidated, rough and heavly lineated region with minimal bouldering. Borders Hathor and requires anaglyph

of the region to identify topographic differences. Separated from Ma'at by showing only limited dust cover.Oriented lineamints.

– *Hatmehit*: well-defined depression in the head region that appears to be filled with fine-grained smooth material overlain by a talus. Curvilinear ridge traversing the depression floor.

Summarizing, on the illuminated surface of 67P comet there are 19 regions, outlined by the OSIRIS images. The nucleus displays morphological diversity, classified as consolidated areas, non-consolidated regions, and large irregular depression. The first zones are the most common on the surface and most of these consolidated regions show variable fractured material, which may indicate a very low density, heterogeneity of composition and physical parameters. On the contrary, non-consolidated terrains show smooth planes and dust covered regions. They occasionally contain many boulders and they can be considered as current or past activity regions. Finally, the three large depressions, Hatmehit, Nut and Aten, display physical and morphological features that are difficult to relate with an impact: they may represent regions of massive activity or other endogenic processes.

2.1.2 Gravitational slopes, geomorphology and material strength

There ia a connection between the nucleus gravitational slopes and surface morphology, and this relation provides constraints on the nature of the cometary material and its dynamical properties like tensile, shear and compressive strengths. The slopes of 67P cover a range from 0° to 90° and depending on wether material is consolidated or not, the strength changes: for unconsolidated material, the strength might be scale invariant, while for consolidated material the strength follows a d^{-q} power-law, where d is the scale and q is the power-law exponent , that is equal to 0.6 for water ice [30]. The fractures and features on the 67P nucleus vary from kilometers to millimeters scale and the strength of material can change by three orders of magnitude. Assuming a uniform density inside the nucleus, and referring to El-Maarry et al.(2015a)[7] for the definitions of the regions, five of these areas can reproduce the different morphologies observed on the surface: Imhotep is a region with a wide variety of terrains, Ash is mostly covered by dust and with debris fields made of boulders, Seth is a region dominated by circular depressions, Hator is characterized by cliffs, and Agilkia is a super-region with a large depression of 800 meters width. Each region shows a different gravitational slope, related to a unique morphology and topography. If the gravitational slope angle shows a peak means that there is an overall flatness

of the terrain. Secondary peaks or other bumps are symptoms of steep walls or smooth terrains. In particular, Groussin. et al. (2015) [13] reveal that from 0° to 20° the gravitational slopes is related to terrains covered by a spatially unsolved material, made of particles smaller than 20 cm. Terrains with slopes on the range of 20-45° are consolidated and with boulders from 1 to 10 meters diameter. High-slope terrains in the range of 45-90° are characterized by cliffs with consolidated material and any boulders on surface.

2.1.3 Tensile, shear, and compressive strength of the cometary material

For a given material can be identified three types of strength: the tensile strength σ_T, the shear strength σ_S, and the compressive strength σ_C. This stregths define the ability of a material to withstand mechanical stresses. Usually, $\sigma_T < \sigma_S < \sigma_C$ and they depend on the scale at which they are measured.

Tensile strength

The tensile strength can be estimated from overhangs if the following condition is performed:

$$\sigma_T < 3\gamma(L^2/H) \tag{2.1}$$

where γ is the unit weight measured in Nm^{-3}, L is the length in meters of the overhangs, and H is the height in meters of the overhangs. If ρ is the density of the cometary material and g is the local gravity, the above equation can be written as

$$\sigma_T < 3\rho g(L^2/H) \tag{2.2}$$

Groussin, et al. (2015) derives that on 67P nucleus the length and the height of the largest structure are L=100m and H=30m. If g=2x10^{-4} m/s^2, this gives an uper limit for the tensile strength $\sigma_T < 94$Pa.

Shear strength

If *theta* is the slope angle on which the boulder is located, m is the mass in kg of this boulder, and A is the contact area measured in m^2 of the boulder with the terrain underneath, the shear strength can be calculated as

$$\sigma_S = mgsin\theta/A \tag{2.3}$$

and it results from friction and cohesion. For a boulder of radius r, $A = \pi(rcos\phi)^2$, and equation 4.8 becames as follow:

$$\sigma_S = (4/3)\pi r^3 \rho g sin\theta / \pi(rcos\phi)^2 = 4r\rho g sin\theta / 3cos^2\phi \tag{2.4}$$

The shear strength is constrained by the highest gravitational slope $rsin\theta$ value, and for 67P the highest value is equal to 5.2 meters and it corresponds to a boulders with radius r=11.5 m located on a gravitational slope of $\theta = 26.8°$. Assuming a contact area A of 1% of the total boulder surface, defined with $\phi = 80°$, it is obtained a shear stregth $\sigma_S = 22$Pa. In general, for the 67P the σ_S is mist likely in the range 4-30Pa.

Compressive strength

The compressive strength of the 67P nucleus can be estimated from the footprints left by the lander Philae as follow:

$$\sigma_C = F/A = (1/2)mv^2/dA \tag{2.5}$$

where F (N) is the forced applied to a surface of area A (m^2), m (kg) is the mass of Philae, v (ms^-1) is the lander impact velocity, and d (m) is the depth at which the lander penetrated the surficial material. With a mass of 100 kg, an impact velocity equal to the escape velocity of the comet, $1ms^{-1}$, and a contact area of 0.016 m^2, the compressive strength results of 15.6 kPa for the surface material.
In general, the compressive strength of a consolidated material is larger than its tensile strength by usually one order of magnitude, and for this reason $\sigma_C \simeq 10\sigma_T$ [35]. The range of a the compressive strength on 67P stands in the range 30-150 Pa.

Summarizing, the strengts on the 67P are low and the cometary material can be considered as weak. This may help to understand some surface morphologies: the vapour pressure of the gas inside the nucleus exceedes 1 kPa when the temperature is higher than 55 K for CO and 155 K for CO_2, and this means that the CO and CO_2 gas pressure may exceed the compressive strength and the gas may push the sourrounding material, during its path, to the surface. This process contains some unsolved issues, it is not yet clear how solar energy penetrates meters below the surface, despite the low thermal of 10-50 $JK^{-1}m^{-2}s^{-0.5}$. The fragmentation process, the boulder distribution and the presence of fractures on the surface may help to solve this issue.

2.1.4 The CO_2 to H_2O ratio on the comet coma

The study of the coma's chemical contents allows to understand the composition of it and it also reveals the gaseous species distribution on the cometary surfaces and sub-surfaces. Comets are mainly composed by ices, and in particular water (H_2O) and carbon dioxide (CO_2) ices. The Philae lander dispatched on 67P surface and remote sensing instruments onboard Rosetta investigate the inner come and they show that water ice tends to sublimate when illuminated by the Sun, while carbon dioxide shows a different behaviour. Thanks to VIRTIS (Visible, Infrared and Thermal Imaging Spectrometer) infrared observations of the 67P coma, it is observed that water emission seems to be concentrated on the neck regions. In contrast, CO_2 sublimate from both illuminated and non illuminated regions of the nucleus. Observations with ROSINA, Rosetta Orbiter Spectrometer for Ion and Neutral Analysis, at a heliocentric distance of 3.5 AU, revealed that the water sublimation is higher at positive latitude regions, while at the winter hemisphere corresponding to negative latitudes, CO_2 emissions are more intense. The CO_2 abundance value is between 2.5% and 80% relative to water, and this is due to a seasonal effects [26].
The spectra observed by VIRTIS show H_2O and CO_2 emissions at 2.6-2.76 μm and at 4.2-4.3 μm respectively, superposed over a continuum, which is mainly due to scattering from the dust at short wavelengths. The band area (I) is converted in column density (N) adopting the g-factors (g_f) at 1 AU equal to 3.349x10^{-4} s^{-1} for H_2O and 2.86x10^{-3} s^{-1} for CO_2. The two quantities are related through the following equation

$$I = (h\nu/4\pi)g_f(1/R^2)\langle N\rangle \tag{2.6}$$

where N is in m^{-2}, I is in W m^{-2}, ν is the central frequency of the band and R is the heliocentric distance in AU.
The variability of H_2O and CO_2 emissions might reflect differences in composition of the cometary surface, but it can be also related to different illumination conditions. In the case of 67P comet, the maximum CO_2 emission is reached in the southern hemisphere, at longitude 353° and latitude 23°S, and it is located in the Hatmehit-Bastet region. Water emission is ten times more intense in the Seth-Hapi region and these behaviours trend as a function of distance from the nucleus. The CO_2/H_2O ratio increases away from the nucleus because the water content decrease more rapidly than carbon dioxide. This investigation reveals that the CO_2 band emission, centered at 4.27 μm, is on average 10^{19} molecules s^{-1} and the column density is weak above the neck region, while it is diffused in the head and the Southern regions. This behavior seems to reveal that CO_2 emission is not strongly related to the

solar illumination, unlike for the case of water ices. A second local maximum of CO_2 emission is located at the border of Imhotep region.

2.1.5 Morphology and dynamics of the cometary activity

The outgassing process on the 67P nucleus is higly anisotropic and the investigation of the development of this effect, as the comet approaces to the Sun, is due to OSIRIS images. From these observations, it appears that jets structure changes in dimension and collimation, and this time variability could be caused by the diurnal variation of solar insolation conditions, and by the related variations of the surface temperature, or by geometrical conditions. The outgassing process can be thought of nature transient and it is controlled by some on- and off-mechanisms, such as the gas source has become extinguished, as the surface temperature changed. The importance to study the jet dynamics and the morphology is to identify the source regions of the gas and dust emission. Lin, Z, et al.(2015) [22] found that the jets most likely emerge from the central part of Hapi, as shown in figure 2.3. The anisotropic morphology of the dust jets is related to the confinent effect of the two lobes of the comet and it is possible the presence of differences between the composition of the dust grains and the surface material on Hapi and the rest of the nucleus.

The detection of water and little carbon dioxide vapor above the active source region in the neck from VIRTIS, and the numerous mini-outburst in Seth region driven by CO/CO_2 sublimation, might be indicative of differences in the source mechanism and chemical composition. Furthermore, the excess total brightness of the collimated of 3-10% with respect to the dust coma, means that the dust grains emitted from the neck region might be subject to fast sublimation, acceleration or fragmentation.

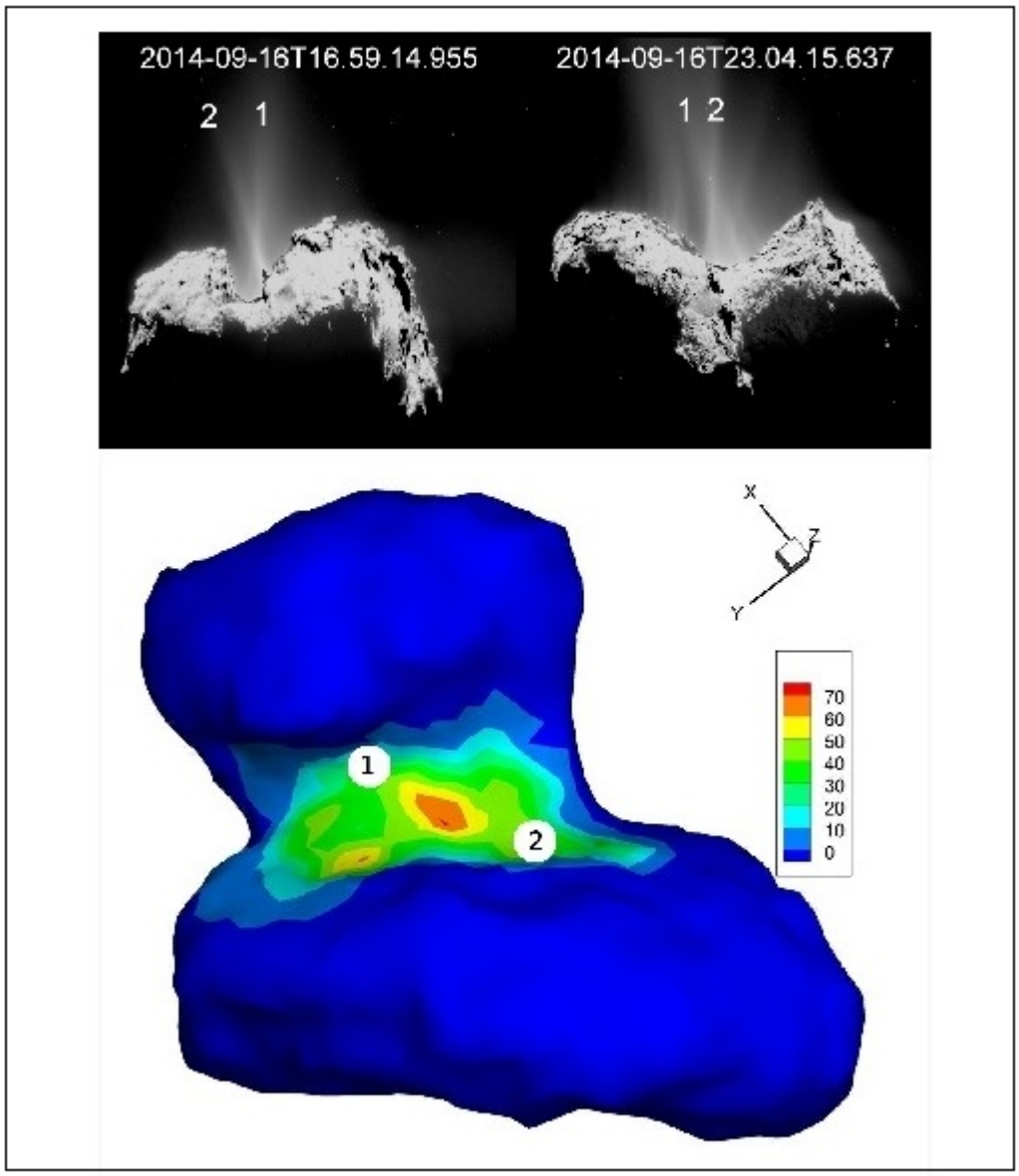

Figure 2.3: Locations of the potential source regions of the jets emitted from the neck region. Spots 1 and 2 are the possible locations of the two jets referred to as jets 1 and 2 on September 16, 2014 (top panel). The color bar indicates the most likely distribution probability of the numerous jets identified in different images [Lin, Z. et al(2015)].

Chapter 3

Fragmentation and boulders distribution

In this chapter will be analyze the fragmentation process by a physical point of view and it will be connected with the size- frequency distribution of the boulders on 67P surface.

3.1 Fragmentation process

The fragmentation is the breakage of a contiguous body into several pieces and it occurs in very distinct contexts and at any scale: from the DNA fragmentation controls cell replication to a supernova results from the fragmentation of giant stars. At the most foundamental level, it may also help to recount the hystory of the Solar System.
The physical mechanisms underlying the dynamic fragmentation are explored to numerical simulation, and the finite element method with dynamic insertion of cohesive elements constitutes the basis of the serial calculation. This process is very violent and the scientists began by studying the results of fragmentation, i.e. the number and the size of fragments. All fragmentation models are well represented by the distribution of the fragment sizes as a power law. Furthermore, the fragmentation is a non-instantaneous precess in which dynamical effects prevail. Instead of considering fragmentation through its dynamical effects, the geologist Grady formulated an expression of the fragment size, based on loading rate and relevant material properties [11]: his law predicts the number of fragments resulting from the fragmentation of a one-, two-, and three-dimensional structure.
Dynamic fragmentation is based on complex precesses which may be classified in three stages: crack nucleation, crack propagation and fragment coa-

lescence. They infer distinct physical mechanisms based on material defects, dynamic of stress waves, and energetic arguments.
The nucleation phase depends on density and size material defects, on the rate and duration of driving force; this phase determines the number of initiated cracks and when a crack is activated, it makes the stress decrease locally to zero. This stress alters the sourrounding areas through stress waves that propagate in every direction.
The second step is crack propagation: a crack propagate and grows until it reaches a free surface, or untill the stress intensity factor falls below a critical threshold. Crack orientation depends on the direction of the tensile stress and may deviate from the nominal path because of the presence of material heterogeneities, and because of sourrounding crack states.
Finally, understanding crack coalescence, forming fragments of different sizes and shapes, is crucial in determining the distribution of fragment sizes.

Figure 3.1: Shattering of a glass and artistic representation of the fragmentation of an asteroid.

The aim of studying the fragmentation processes is to determine the relation among the number of initiated cracks with the density and the size of material defects, and the rate and the duration of the driving force, so to better understand the dynamic of fragmentation and the propagation of cracks. The application of fragmentation theory on boulder distributions as determined by the analysis of the OSIRIS images of cometary surface, would allow to understand the processes underlying their formation and thus the evolution and structure of comet itself.

3.1.1 Physics-based fragmentation

Wave propagation and characteristic length

Let us consider a material to be perfectly plastic with yield strength Y, and assuming that failure is an instantaneous process at the breakpoint location [11]. This caused a non-linearity in the stress field, which results in stress waves propagating from the breakpoint to the surrounding areas. These regions suffer tensile stress lower than Y are rigid, and the boundary between rigid and plastic zones is located at the position X relatively to the breakpoint:

$$X(t) = \sqrt{2Yt/\rho\dot{\epsilon}} \tag{3.1}$$

where ρ is the volumetric mass and $\dot{\epsilon}$ is the constant strain rate.
The velocity of the crack propagation depends on material (Y,ρ) and kinematic ($\dot{\epsilon}$,t) parameters.

Statistical description of the event of fracture and average length scale

The occurrence of fracture is governed by the fracture frequency $\lambda(\epsilon)$ and the probability that fractures occurs in a length dl at strain ϵ is $\lambda(\epsilon)d\epsilon dl$. The length scale emerging from the statistical fragmentation theory of Mott is

$$\mu = \sqrt{2Y/\rho\epsilon^2\gamma} \tag{3.2}$$

where γ is the scale parameter in $\lambda(\epsilon)$ function.
This function $\lambda(\epsilon)$, also called *hazard function*, is focused on three forms [27], respectively exponential, Weibull and Gumbell distribution:

$$\begin{aligned} \lambda(\epsilon) &= \lambda_0 \\ \lambda(\epsilon) &= (n/\epsilon_0)(\epsilon/\epsilon_0)^{n-1} \\ \lambda(\epsilon) &= Ae^{\gamma\epsilon} \end{aligned} \tag{3.3}$$

where n is a characteristic constant, in particular n$\geq$ 1.

Let us now consider a line in which breakpoints are induced randomly and the failure sequence follows a Poisson point process, i.e. events occur continuously and indipendently of one other. Taking into account the limiting grain size of a body, it is possible to determine the minimum spacing between two breakpoints [11]. If the minimum size is δ, the number of of breakpoints per unit length in N=$1/\delta$ and if N_f is the number of fractured sites, the probability of fractures at any breakpoint is p=N_f/N=δ/N_f. The probability of finding an element of length l=nδ is P(l)=(1-p)^{n}p.

3.2 Boulders distribution on 67P surface

The nucleus, its activity, and the surface morphology of 67P, as observed from OSIRIS cameras, are described with a very high resolution: one of the interesting features on the comet surface is the ubiquitous presence of large boulders. i.e. positive reliefs detectable in different images with the constant presence of elongated shadows whose extension depends on the illumination geometry, and that seem to be detached from the ground where they stands. On asteroids and planets are usually observed several boulders of various size, the largest fragments excavated by the collision resulting from surficial impacts. In this case, the impact formation process is not sufficient to explain the presence of boulders, mainly considering that no evident impact crater has been recognized up to now on 67P surface.

3.2.1 Boulder formation processes

The boulders can be found both isolated or in clusters, and they are located at the basis of scarps or depressions. Obviously, this distribution depends on the different formation process and evolution they have undergone and, as the surface is active and a changing environment, multiple formation processes are expected to be at work. The most likely processes are the thermal stress fragmentation, gravitational phenomena, jets, activity and possibly impacts.

Thermal stress and sublimation

Thermal stress occuring on the comet surface allows the formation of dislodged blocks from cracks and fractures, and this occurs on the comet surface through changing insolation conditions and it is controlled by solar illumination (diurnal cycle) with the rotation period of the comet of 12,761 h, and with seasonal variation (summer and winter hemisphere). The images reveal a clear dichotomy between the northern and southern hemisfere, in fact the northern one is weakly illuminated when the comet is far from the Sun; in contrast, the southern in strongly insolated during the short perihelion passages. Fragmentation by thermal stress is related also to the sublimation activity, in fact the boulders are made of dust components mixed with ices and volatile materials: when the comet approaches the Sun, the surface is affected by sublimation and consequently fracturing. These are the main causes that increase the number of smaller boulders with respect to the larger blocks, reducing the smaller boulders into dust. In 2015 Pajola et al. derived the size-frequency distribution of boulders on a comet 67P, finding

that the thermal stress results in a steepening of the size-frequency slope, while sublimation tends to make the slope fainter.

Gravitational phenomena

Gravitational phenomena are the dominant process on 67P and they are induced by differential erosion. The comet surface is characterized by numerous scarps, dominated by niches and terraces, and at their bases can be found localized debris fields. The sublimation plays an important role because a differential erosion is connected to the different content of material disposed to volatilization: in fact, the erosion is higher for material inclined to volatilization. If a layer starts sublimating, the collapse of the uppermost strata is favorite. These deposits not only underwent a period of sublimation, but also the comet activity is very important for this phenomena: in fact, if an outburts occurs, some of boulders can be lifted and it can erode the surrounding area favoring new gravitational collapses.

Activity and lifted boulders

As discussed before, the boulders can be found isolated in several locations on the 67P surface. This fact is due to the cometary activity and its jets: these boulders are lifted by outgassing after a former fragmentation. The dimension for a boulder that can be lifted from the surface is calculated considering the local surficial gravity field, the centrifugal force and the drag force producing by the outgassing: if M_b is the mass of the boulders, a is the acceleration, s the radius of the boulder, v_g the gas velocity ($\simeq 1km/s$), r the cometocentric distance and $(dm/dt)_g$ is the gas-loss rate, through Stokes can be computed the gas drag force [9]

$$F_{Dg} = M_b * a = (C_D s^2 v_g / 2r^2)(dm/dt) \tag{3.4}$$

When the drag force is similar to gravity, the boulder can be lifted. Larger boulder size that can be lifted by cometary activity, expressed as $(dm/dt)v_g$, is between 2 and 6 meters.
Considering a lifted boulders, another important aspect related to the boulder distribution is the subsequent impact after the lifting process. A possibly further fragmentation depends on the velocity and porosity of the mass. The breakup velocity was studied by Beitz et al. (2011) [2], considering a tensile strength of 1000 Pa

$$v_{break} = \sqrt{(4 * (T/10000Pa)^{0.75} * (s/34micron)^{-0.95})} \tag{3.5}$$

where T is the boulder's tensile stregth, s is the boulder diameter. Considering velocities between 0.1 m/s and 0.9 m/s, similar to escape velocity ($\sim 1m/s$), the boulders larger than 10 cm break for a strength of 10000 Pa.

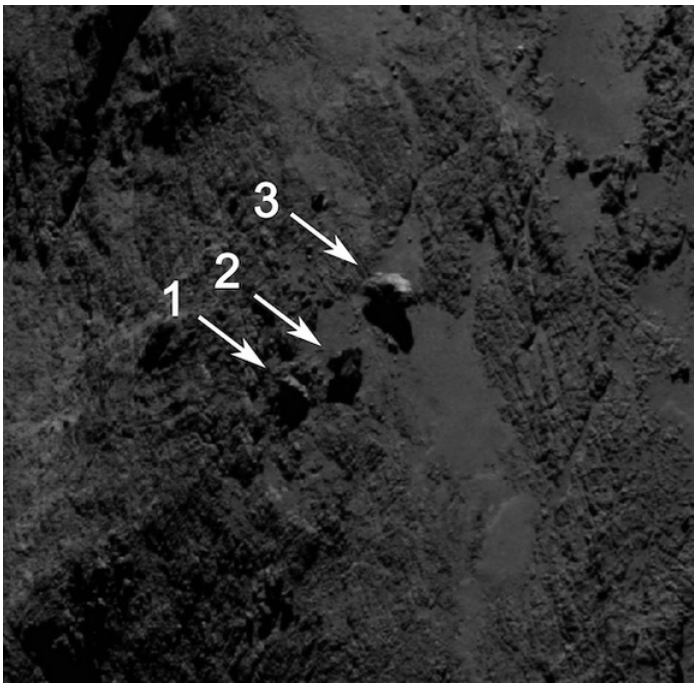

Figure 3.2: Example of boulders on comet 67P/C-G. This image was taken by OSIRIS on September 2015.

3.2.2 Size-frequency distribution

Pajola et al. (2015) analyzed the boulders distribution on the 67P surface. They considered diameter larger than 7 meters and this value derives from the images with the lowest resolution. The global distribution of the boulders shows that these objects are ubiquitous on the nucleus, but the larger of them are located in the region between the two lobes, called the neck, and in the Imhotep region. The cumulative boulder size-frequency distribution per km^2 over the illuminated side of the comet was derived considering a surface area of 36.4 km^2 [34]. The power-law index value is -3.6+0.2/-0.3.

After that, they performed the same analysis by considering the body, the head and the neck as separate regions of the comet in order to find some differences in the previously size-frequency distribution. Specifically, the body has an illuminated surface of 22.5 km^2, the head of 10.8 km^2, while the neck alone covers 3.1 km^2. The cumulative total number of boulders is 3546, in

particular 2218 on the body, 1115 on the head and 213 on the neck. The results are listed in Table 3.1.

Name	Area [km^2]	Tot N boulders $\geq$ 7 km	7m boulders per km^2	Power-index	+	-
All	36.4	3546	97	-3.6	0.2	0.3
Body	22.5	2218	99	-3.5	0.2	0.3
Head	10.8	1115	103	-4.0	0.3	0.2
Neck	3.1	213	69	-2.2	0.2	0.2

Table 3.1: Names and area of different regions, total number of boulders $\geq$ 7m, surface density, power-law index, associated error.

The total number of boulders with a diameter larger than 7 meters is similar for the body and the head of 67P, in fact there are almost 100 boulders per km^2. The neck differs from these two regions and in particular there are only 69 boulders per km^2. Recent studies reveal that there are not mineralogical difference between the two lobes and the neck [Capaccioni et al. 2015], and the formation processes are the same. The differences in the size-distribution power-law are related to the fracture density of the surface in which these boulders are detached. A higher power-law index probably means a more surface fracturing, and for these considerations, the head is more fractured than the body of the comet. The trend of the neck, called Hapi, needs another explanation. The OSIRIS images analized reveal three possibly scenarios for the boulder formation on the neck region: first of all, the neck is the most active region of the northern hemisphere of 67P and its activity could be the reason for the slow cumulative size-slope, because the boulders are completely destroyed and sublimated. The second possibility is that the small boulders located on the neck derived from other regions, like Hator and Seth, or that the smaller boulders could have been lifted up from the neck and been redistributed or dispersed away from the comet.

The same analysis was made on localized areas and in particular they identified two regions on the body, which consist of three areas that are representative of the layered or niche region of Seth and Ash, and a region with one depression on Ash, a smooth region inside Imhotep and a layered region in Khepry.

Body region 1 size-frequency distributions: Seth/Ash is a layered region with niches and cliffs, layered terrain dominated by terraces covered with smooth deposits. This region listed above have a distance from 67P center of 117.15 km, a scale of 2.18 m/px and a phase angle of 50.81 degrees.

Geographical unit	Area [km^2]	Boulders [N/km^2]	Power-law index	Diameter [m]
Seth/Ash	4.96	100	-4.2	>7

The Seth/Ash region shows different niches and large terraces covered by smooth layered terrain with deposits of boulders. The slope of this area with a power-law index of -4.2, lower than the specific pit location, is probably due to gravitational processes and no activity or sublimation processes.

Body region 2 size-frequency distributions: in these areas are visible a smooth region, a layered region with niche and terraces, and a wide elongated depression. The first area is located within the smooth region of Imhotep and deposits of boulders are close to scarp and depression, while a flat area without boulders is located on the right side of the depression. Imhotep is a smooth background dominated area, Khepry/Ash is a layered region with large niches and 2-step like terraces with gravitational deposits, and Ash is a wide elongated depression with talus deposits at its base.
Imhotep, Khepry/Ash and Ash are distant 113.45 km to the center of the comet, the scale is 2.11 m/px and they have a phase-angle of 47.03 degrees.

Geographical unit	Area [km^2]	Boulders [N/km^2]	Power-law index	Diameter [m]
Imhotep	0.19	485	-3.6	7-11
Khepry/Ash	0.29	385	-3.8	>7
Ash	0.16	769	-6.4	>7

The whole Imhotep area could have undergone to sublimation and erosion at the cliffs. The results could be interpreted as an elimination of the smaller boulders in the central part of the depression and an erosion of the sourrounding parts.

Head size-frequency distributions: a gravitational deposit inside Nut and the circular depression Hatmehit are analyzed in the head of 67P. The rim of the depression shows collapses and fracturing, but the floor is smooth and flat. Nut shoes gravitational deposit inside a depression, Hatmehit is almost circular depressions with evidences of large scale collapses and fracturing. The distance of these regions frome the center of the comet is 131.5 km, the scale is 2.41 m/px and the phase-angle is 50.14 degrees.

Geographical unit	Area [km^2]	Boulders [N/km^2]	Power-law index	Diameter [m]
Nut	0.17	424	-3.9	>7
Hatmehit	0.49	350	-3.4	7-13

Other analyzed regions: Hator has fractured cliffs, it is distant 81.57 km from the center of the comet, the images have a scale of 1.54 m/px and the phase-angle is 34.33 degrees. Aswan is a terrace covered with some smooth gravitational deposits above and below the cliffs area, its distance is above 28.4 km, the scale is 0.50 m/px and the phase-angle is 72.04 degrees. Finally, Abydos is an unconsolidated talus deposit and it is distant 20.25 from the center of the comet. The resolution is 0.34 m/px and the phase angle is 90.92 degrees.

Geographical unit	Area [km^2]	Boulders [N/km^2]	Power-law index	Diameter [m]
Hator	1.81		-5.2	7-18
Aswan	0.68	1499	-3.9	2-8
Abydos	0.02		-4.0	>1.7

Comparing the power-law index and the morphology of these regions, the conclusions are that high fractured zones are characterized by a high power-law indices of about -5 to -6.5, with collapses and pit formation, with depression and subsequent escape of volatiles. Indeces of -3.5 and -4 are a markers for gravitational events due to sublimation or thermal stress, causing regressive erosion. Finally, material formed during gravitational phenomena or collapsing, and not renewed, are characterized by a power-law indices of -1 and -2.

Chapter 4

Thermal insolation and boulder distribution on comet 67P/Churyumov-Gerasimenko

From the analysis of the CO_2 to H_2O ratio, the 67P comet appears as a very peculiar bilobate objects: the comet head receives the maximun solar flux at a heliocentric distance of 2 AU, while the big lobe is fully illuminated during the perihelion passage at 1.2 AU. The 67P spin axis orientation respect to the orbital plane implies that a large portion of the surface is never illuminated for a long period time. All of these characteristics are driving the activations of the volatiles sublimation occurring in different places of the surface.
As shown in the description of the gravitational slopes of the 67P nucleus, there is a large presence of boulders on slopes lower than 20° and these objects are usually isolated, far from high-slope terrains and too large to be lifted by gas drag. Another ideas is that these boulders are leftovers from previous basins and depressions. On Seth region, the boulder fields end on slopes lower than 20° and they could be the result of progressing eroding process of the nucleus. The small degradation involves fractal fragmentation into small pieces, and this process can explain the presence of fine material on the boulder fields. Terrains steeper than 20° are covered by dust and could be ancient boulder fields affected by degradation process of cliffs and boulders.

In this chapter will be analyzed the connection between insolation, irradiation and boulder distribution on the 67P surface, computing the solar incidence, the phase and the emission angles through an IDL code, and analyzing the related amount of irradiation on the comet surface. A high value

of irradiation on the surface facets leads to a higher sublimation of the ices contained in the cometary material, thus increasing the presence of small boulders than those of larger dimensions.

4.1 Insolation, erosion and morphology of comet 67P

The large obliquity (52°) of the comet and the orientation of the spin axis causes strong seasonal effects on the cometary surface and leads to a dichotomy. The southern solstice occurs only 34 days after perihelion at a heliocentric distance of r_h=1.24 AU. For this reason, the northern solstice is reached after perihelion, at r_h=5.68 AU. The equinoxes are passed at r_h=1.7 AU, before perihelion, and r_h=2.6 AU after perihelion. The results are that the northern hemisphere is relatively weakly illuminated for a long time, when the comet is far from the Sun, whereas the southern hemisphere is strongly insolated during the short perihelion passage. The region between the two lobes, the neck, is low insolated because this area is shadowed by the lobes for most of the spin period. The analyses of the diurnal insolation conditions are relates to the sublimation and insolation model, knowing that sublimation of volatiles requires insolation and this depends on the surface temperature. The termal inertia of the comet is between 10 and 50 J m^{-2} K^{-1} $s^{-1/2}$ [14], and this low value requires a very low thermal conductivity, in the range of 10^{-4} to 10^{-3} W m^{-1} K^{-1}. Obviously, the asymmetry of the seasonal and diurnal insolation influences the shape and the morphology of the comet.

4.1.1 Insolation and sublimation model

The irregular shape of the comet is considered as a polyhedron made of triangular facets, as required by Tassellated Plate Model, shown below. The amount of insolation of a single facet is derived considering its orientation with respect to the Sun. In addiction, the energy balance of the comet is affected by mutually facing facets and by their thermal IR radiation, resulting in a local flux enhancement in the presence of concavities. This thesis does not include these effects of self-illumination, because the primary objective of this work is study the rule of the direct insolation and irradiation on a single facet.
Sublimation depends not only on the amount of insolation, but also on the intensity of insolation. The energy absorbed by the cometary surface after the direct insolation, can be used to sublimate volatiles on or under the

surface, an the related thermal stresses can fracture the surface producing fractures and blocks like boulders. In a sublimation model, the assumption is that exposed water ices sublimates directly from the surface. If

$$P = 3.56{\cdot}10^{12} exp(-6141.667/T) \tag{4.1}$$

is the water vapor pressure in [kg m^{-1} s^{-2}], and

$$v = 8RT/\pi\mu \tag{4.2}$$

in [m s^{-1}], with R the gas constant and μ the molar mass of water, is the thermal velocity, the sublimation rate is given by the Hertz-Knudsen formula

$$Z(T) = 2P(T)/(\pi v) \tag{4.3}$$

The water ice on the surface is covered by a dust layer and this has to be thin enough to pass the solar irradiation and fragile enough to be removed by the vapor pressure.
All models of cometary nucleus formation lead to a porous mixture of ices and dust, and a very low tensile strength of the comet material. The amount of energy available for sublimation depends on the heat conductivity through the dust layer, and this includes the conductivity through solid medium and inside the pores of the material, considering the medium as a hierarchic structure composed by porous layers consisting of porous aggregates. Through $Z(T)$ is possible estimate the local erosion rate at a specific surface element as follow

$$\Delta x/\Delta t = Z(T)/\rho \tag{4.4}$$

with ρ density of considered ices in the nucleus. ΔT is the time step over which Z(T) stays constant.
Considering the total insolation ad sublimation, and the dicothomy of the comet nucleus, it is shown that only about 25% of the maximum erosion is reached on the northern hemisphere, while the total insolation reaches the 80%: there is not a linearity of sublimation with temperature [18]. The dichotomy of erosion between the northern and southern hemisphere of 67P is very unique: the south side is eroded uniformly by close 4 meters per orbit. The northern side erodes much less rapidly and the equatorial areas, inclined towards the south, are well eroded and displays a smoother topography than the north.

In view of all this, the purpose of this thesis is compute the amount of solar irradiation on different areas of the 67P surface, the same regions in which there are boulder distributions. What we expect to find is that in

regions with a high absorbed heat, the number of small boulders is higher than region with a low thermal irradiation, and this because the solar heating induces the sublimation process of ices. The study begins knowing that the southern summer of the comet is very intense around perihelion and 3/4 of all eroded material is lost during this season.

4.2 The termophysics of boulders on surface 67P

In order to understand the boulder deposit on 67P surface, it is very important to determine the thermophysical processes in the surface layers of the nucleus. The crack and boulder formation in the nucleus is enhanced by high temperature fluctuations and they are induced by thermal stresses due to the low thermal inertia of the surface. The thermal inertia is a property related to thermal conductivity and volumetric heat capacity. A high thermal inertia means that dynamic effects are prevalent in a heat transfer model. In particular, the inertia $I = \sqrt{\rho c \lambda}$ describes the time lag of surface temperature adjustments and depends on density ρ, heat capacity c and heat conductivity λ of the nucleus layers. The scientific camera OSIRIS onboard Rosetta has shown that one of the predominant surface features are boulders, whose processes and evolution are not yet well understood.
The aim of the following work is to figure how solar illumination conditions and thermophysical parameters affect the diurnal sublimation and induce an erosive process.
Thermophysical properties of the comet nucleus can be derived from VIRTIS spectrometer data: it is distinguished between the thermal inertia of local terrain morphologies, as the rougher consolidated material with $I > 50$ J m^{-2} K^{-1} s$^{-1/2}$, and dust layer areas with $10 < I < 25$ J m^{-2} K^{-1} s$^{-1/2}$. The average geometric albedo is 0.059 and the emissivity is 0.97.

In the following analysis, we consider the surface of the 67P comet as a collection of plate triangular facets, each one illuminated by the solar flux with an incidence angle θ between the surface normal and the solar vector. This angle is time-dependent within a diurnal period.
Considering a single node i, the general thermal balance equation is

$$Q_{abs,i} + \Sigma_j Q_{rad,ij} + Q_{con,im} + Q_{con,in} + Q_{sub,i} = Q_{cap,i} \tag{4.5}$$

The j index considers all faces in radiative contact with node i, $Q_{rad,ij}$ is the radiative heat flux between nodes i and j, including the emitted flux to the

deep space boundary node. $Q_{con,in-m}$ is the conductive heat flux between neighbour nodes upper m and lower n, $Q_{sub,i}$ is the heat due to the sublimation process, $Q_{cap,i}$ is the capacitive heat storage and $Q_{abs,i}$ is the heat referred to the absorbed solar irradiation per face i.
The solar irradiation is the major source term of the heat balance of a cometary nucleus and in particular the absorbed solar heat flux of each considered surface element A_i is:

$$Q_{abs,i} = (1-\alpha)(S/(r_h)^2)A_i cos\theta_i(t) \tag{4.6}$$

where α is the albedo, R is the heliocentric distance of comet in AU and S the solar constant at 1 AU. The units are W/m^2.
Actually, the total amount of absorbed solar energy for surface element i is determined by the fraction of exposure time to a whole diurnal period P_{diu},

$$\gamma_{exp}/2\pi = (t_2 - t_1)/P_{diu} \tag{4.7}$$

and the solar heat fluxes depend on terrain morphologies. In fact, the illumination conditions are restricted by the shadowing effects to the rim of fractures, pits or other features. In this case the total amount of absorbed solar energy $E_{abs,i}$ for surface element i is

$$E_{abs,i} = \int_{[t_1,t_2]} Q_{abs,i}dt = \int_{[t_1,t_2]} (1-\alpha)(S/R^2)A_i cos\theta_i(t) \tag{4.8}$$

with the integration limits set by times t_1 and t_2 when the Sun passes both rims, concavity, fractures and the illumination conditions differ for selected areas. These last considerations were introduced in a different way in this thesis, because in this case the integral 4.8 from t_1=2014 August 01, to t_2=2016 July 17, is considered as the total amount of absorbed solar energy about one year before and after the perihelion, i.e. the irradiation in Wh/m^2.

4.2.1 SPICE and the computation of solar irradiation data

SPICE is an observation geometry information system for planetary science missions, in place to plan and to interpret scientific observations from space-based instruments aboard robotic planetary spacecraft. SPICE was builted by the Navigation and Ancillary Information Facility (NAIF), acting under NASA's Planetary Science Division, and it is focused on solar system geometry. The primary SPICE data set, called *kernels*, are composed of navigation and ancillary information, and they contain several packages of data:

- S-Spacecraft ephemeris, given as a function of time (**SPK**);
- P-Planet, satellite, comet or asteroid ephemerides, given as function of time (**SPK**);
- P-Physical, dynamical and cartographic constraints for target bodies, such as orientation of the spin axis and shape specification (**PCK**);
- I-Instrument description kernel, size, shape and orientation of the spacecraft instruments (**IK**);
- C-Poynting kernel, containing C-matrix which provides orientation and pointing angles for a spacecraft and its instruments. A C-spice includes also angular rate data for that structure (**CK**);
- E-Event kernel summarizing mission activities, planned and unanticipated (**EK**);
- **FK** is a frame kernel containing specification for reference frames used by flight projects. This file include also mounting alignment information for instruments and antennas;
- Spacecraft clock (**SCLK**) and leap seconds (**LSK**) kernes are used in converting time tags between time measurement system;
- **DSK** is a digital space kernel both for small, irregular shape bodies such as asteroids and comet nuclei, and for large more uniformly bodies, such as moons and planets.

The SPICE system includes the SPICE toolkit, a collection of libraries and subroutines needed to read the kernel files, and to calculate observation geometry parameters. The toolkit used for this thesis is called *Icy* and it is implemented in IDL language, and the kernels used in the IDL code are referred to ROSETTA mission.

The first step of the IDL code used for this thesis is to load the spice shape model of the target, the 67P/Churyumov-Gerasimenko comet, and to insert the latitude and longitude of the regions useful for this analysis. The Digital Shape Kernel subsystem enables SPICE applications to make use of surface shape data: it handles two particular representations of shape data, like **Digital Elevation Model** (DEM), and **Tessellated Plate Model**. The first representation defines the elevation of a surface point as distance from the center of the considered reference system. The tassellated method splits the surface in a collection of triangles and it is a very flexi method. For

this work it was choosen this second approach.

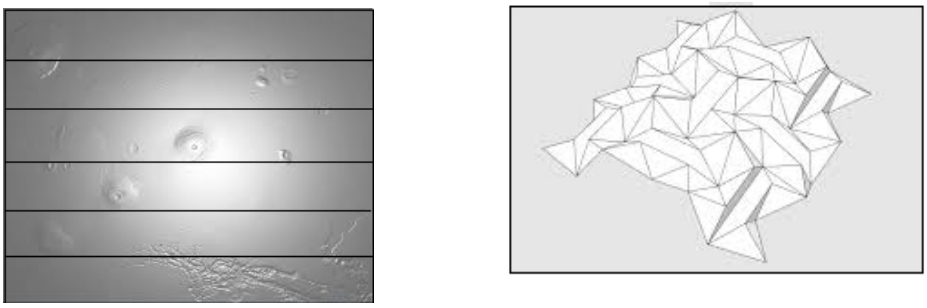

Figure 4.1: In the left side is represented the DEM method, in the right the Tasselled Plate method.

The latitude and the longitude of the selected areas have been chosen in such a way that the points represent the vertices of a triangle, in order to cover the selected area in the best way. These regions were chosen because they are the same as analyzed in the work of Pajola et al.(2015) [29], in which is present an analysis of the size-frequency distribution of boulders. The values are listed in table 4.1 and the units are radians. In the last column there is the area A_i in km^2 of the selected regions.

Regions	Lat	Long	Lat	Long	Lat	Long	A_i [km^2]
Seth/Ash	67	80	60	165	55	190	4.96
Imhotep	-11	115	15	170	-60	190	0.19
Khepry/Ash	10	100	12	110	15	120	0.29
Ash	23	226	20	216	36	85	0.16
Nut	0	320	11	325	21	333	0.17
Hatmehit	10	340	0	0	15	342	0.49
Hator	15	300	30	20	0	30	1.81

Table 4.1: Latitude, longitude and area of the selected comet regions.

In the code have been inserted the values of solar latitude and longitude with respect to the center of the Solar System and it was decided to include the kernels data and the ephemerides of the bodies involved from 01 August 2014 to 17 July 2016, with a step time of one hour. The reason is that Rosetta was launched in 2004 and the spacecraft arrived at comet 67P in August 2014 entering the rendezvous phase, and also this range time was chosen because it represents exactly one year before and one year after the passage of the comet at perihelion, 2015 August 13. The time step of an

our was selected in order to obtain values of phase, emission and solar incidence angles carefully. The 2016 July 17 is the last day in which data for the present work are available. The ephemerides give the position of naturally occurring astronomical objects as well as artificial satellites.

The computation method used in the code is called **INTERCEPT**: in this method the sub-observer point is defined as the target surface intercept of the line containing the observer and the target's center. The target body is treated as a triaxial ellipsoid with a radii available in the kernel pool. The results will be corrected for aberration: **ABCORR** indicates the aberration corrections to be applied to the state of the target body, the comet 67P, to account for one-way light time and stellar aberration. In particular, the **ABCORR=LT+S** is the correction for one-way light time and stellar aberration using a Newtonian formulation. *LT* correction yelds the state of the target at the moment it emitted photons arriving at the observer time '**et**', observer epoch. *et* is the ephemeris time, expressed as seconds past J2000, at which the apparent illumination angles at the specified surface point on the target body, as seen from the observing body, are to be computed. *LT+S* modifies the state obtained with the *LT* option to account for the observer's velocity relative to the Solar System baricenter. The result is the apparent state of the target, its position and velocity as seen by the observer, the Sun. All surface features on the target body will appear in a measurement made at *et* epoch, as they were at the target at this epoch. In particular, lighting on the target body is dependent on the apparent location of the Sun as seen from the target body. In addition to light time correction, stellar aberration is used in computing the apparent target surface point position as seen from observer's location at time *et*. This apparent position defines the observer-target surface point vector.
The target body-Sun vector is the apparent position of the Sun, corrected for light time and stellar aberration, as seen from the target body. The target body's position is not affected by the stellar aberration correction applied in finding its apparent position as seen by the observer.

To continue, it has been inserted the **solar constant** equal to 1361.1 [W/m^2], the mean solar electromagnetic radiation (the solar irradiance) per unit area that would be incident on a plane perpendicular to the rays, at a distance of one astronomical unit (AU) from the Sun. In this case, the constant has been modified in order to consider the real distance of the comet 67P with respect to the Sun, with a perihelion of 1.2 AU, and the final value is computed by

$$\begin{aligned} scost &= 1361.1 \\ al &= 0.04 \\ cs = scost * (1 - al) &= 1306.656 \end{aligned} \tag{4.9}$$

Once loaded all kernel data, the strings representing the start and end time of collecting data are converted to a number of seconds past the J2000 epoch corresponding to the input epoch:

$$\begin{aligned} time_0 = 1 - August - 2014 = 4.06 * 10^8_{sec} = et_0 \\ time_F = 31 - July - 2016 = 5.23 * 10^8_{sec} = et_F \end{aligned} \tag{4.10}$$

Once opened the shape file, a point grid is placed on it including the latitude and longitude of the selected area: these values were in degrees, they are converted first in radians and now in rectangular coordinates to be placed on the grid. The rectangular coordinates are the cartesian coordinates of a celestial body referred to the center of another celestial body

$$\begin{aligned} x = rcos(\theta) \\ y = rsin(\theta) \end{aligned} \tag{4.11}$$

Until now it has been created a grid of dots positioned on the shape file in order to be able to identify the selected area in cartesian coordinates. Once created this grid, it was computed the illumination angles, in particular the phase, solar incidence and emission angles at a specified point on a target body at a particular epoch, corrected for light time and stellar aberration.

The **phase** is the angle between the surface point-observer vector and the surface point-Sun vector. The units are radians and the range phase is [0,π]. This is the angle as seen from observer, in this case the Sun, at time *et*.

Solar is the solar incidence angle on the surface point as seen from the observer at epoch *et*. This is the angle between the surface normal vector at surface point and the surface-point Sun vector. Units are radians and the range is [0,π].

Finally, **emission** is the emission angle at surface point, as seen from observer at epoch *et*. This is the angle between the surface normal vector at surface point and the surface point-observer vector. Units are radians and the range is [0,π].

Usually, phase angles < solar incidence angle + emission angles.

All angles are shown in figure 4.2.

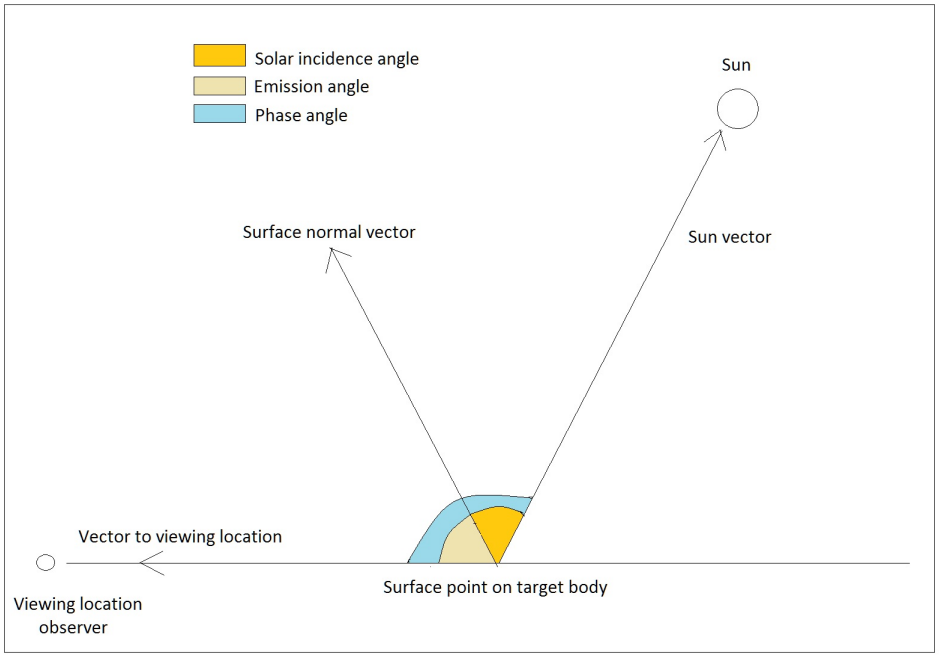

Figure 4.2: General representation of phase, emission and solar incidence angles.

Once computed the phase, solar incidence and emission angles, the ephemeris seconds past J2000 are converted into Julian date format UTC and the rectangular coordinates are referred again into latitudinal reference system. The result is the position of a target body relative to an observing body, corrected for planetary and stellar aberrations, and the heliocentric distance of the target body converted in AU. The three angles are converted from radians to degrees and then it is computed the sub-solar point using a plate model representation of the target's surface. The sub-solar point on a planetary body is where its Sun is perceived to be directly overhead (in Zenith). That is where the Sun's rays are hitting the target exactly perpendicular to its surface.

At this point, the phase, emission and solar incidence angles are computed for each our of the day from 2014 August 01 to 2016 July 17 for all the selected comet regions. As expected the value of incidence and emission angles are equal to each other and this because the surface was choosen as a plate triangular.
In order to compute the heat referred to the absorbed solar irradiation, the values of the comet heliocentric distance and of the solar incidence angle were

averaged over six month, in order to have an insolation trend twice a year, following the strong variations of seasonal effects.
It is important to emphasize that in this thesis the difference between insolation and irradiation is defined as follows: the *irradiation* is the power per unit area received from the Sun in the form of electromagnetic radiation. The *insolation* is the power received on a body per unit area on a horizontal surface integrated over time. Units are respectively W/m^2 and Wh/m^2.

The values are listed in table 4.2, in which are indicated the data range, the comet heliocentric distance in AU and the solar incidence angles in degrees.

Finally, the heat referred to the absorbed solar irradiation per area A_i is computed through the following equation

$$Q_{abs,i} = (1-\alpha)(S/r_h^2)A_i cos\theta_i(t) \tag{4.12}$$

if $\cos\theta > 0$, otherwise $Q_{abs,i} = 0$ if $\cos\theta \leq 0$.
In the case of comet 67P, the albedo $\alpha = 0.059$, the solar constant $S = 1306.656$ [W/m^2], r_h is the heliocentric distance of the comet in AU and θ is the incidence angle in degrees. The results are listed in table 4.3.

At least, in table 4.4 are the insolation values compared with the absorbed heat flux Q_{abs}, the power-law index and the size-range of the considered boulders of different comet regions. The insolation, i.e. the total amount of absorbed solar energy , then is:

$$I = \int_{[t_1,t_2]} Q_{abs(t)}dt = \int_{[t_1,t_2]} (1-\alpha)(S/r_h^2)A_i cos\theta_i(t)dt \tag{4.13}$$

where t_1=et0 in hours, and t_2=etF in hours. Units are [Wh/m^2].

Region	Data	r_h [AU]	Incidence [deg]
Seth/Ash	2014 AUG 01 2014 DEC 31	3.1581966715	115.15750828
	2015 JAN 01 2015 JUL 31	1.8732186722	87.131889812
	2015 AUG 01 2015 DEC 31	1.5219320776	64.183958781
	2016 JAN 01 2016 JUL 17	2.7456273938	97.340442522
Imhotep	2014 AUG 01 2014 DEC 31	3.1581966715	75.787835157
	2015 JAN 01 2015 JUL 31	1.8732186722	91.41014286
	2015 AUG 01 2015 DEC 31	1.5219320776	103.68460159
	2016 JAN 01 2016 JUL 17	2.7456273939	88.2224674
Khepry/Ash	2014 AUG 01 2014 DEC 31	3.1581966715	104.91242362
	2015 JAN 01 2015 JUL 31	1.8732186722	88.594470759
	2015 AUG 01 2015 DEC 31	1.5219320776	75.586694365
	2016 JAN 01 2016 JUL 17	2.7456273938	95.996591073
Ash	2014 AUG 01 2014 DEC 31	3.1581966715	111.7494192061
	2015 JAN 01 2015 JUL 31	1.8732186722	87.5557981788
	2015 AUG 01 2015 DEC 31	1.5219320776	68.0199437955
	2016 JAN 01 2016 JUL 31	2.7456273938	96.3909007045
Nut	2014 AUG 01 2014 DEC 31	3.1581966715	76.089201751
	2015 JAN 01 2015 JUL 31	1.8732186772	91.307357283
	2015 AUG 01 2015 DEC 31	1.5219320776	103.48782684
	2016 JAN 01 2016 JUL 17	2.7456273938	85.532642587
Hatmehit	2014 AUG 01 2014 DEC 31	3.1581966687	106.473962118
	2015 JAN 01 2015 JUL 31	1.8732186722	88.3421588819
	2015 AUG 01 2015 DEC 31	1.7258096361	31.0251871043
	2016 JAN 01 2016 JUL 31	2.7456273938	246.6891556256
Hator	2014 AUG 01 2014 DEC 31	3.1581966714	110.61109023
	2015 JAN 01 2015 JUL 31	1.8732186722	87.6997083686
	2015 AUG 01 2015 DEC 31	1.5219320776	69.3688150742
	2016 JAN 01 2016 JUL 31	62.7456273938	96.1159535948

Table 4.2: Semi-annual values of heliocentric distance and incidence angle of 67P regions.

Region	Data	Area [m^2]	Q_{abs} [W/m^2]
Seth/Ash	2014 AUG 01 2014 DEC 31	4.96 10^8	0
	2015 JAN 01 2015 JUL 31		8.70 10^9
	2015 AUG 01 2015 DEC 31		1.15 10^{11}
	2016 JAN 01 2016 JUL 17		0
Imhotep	2014 AUG 01 2014 DEC 31	1.9 10^7	5.75 10^8
	2015 JAN 01 2015 JUL 31		0
	2015 AUG 01 2015 DEC 31		0
	2016 JAN 01 2016 JUL 17		9.61 10^7
Khepry/Ash	2014 AUG 01 2014 DEC 31	2.9 10^7	0
	2015 JAN 01 2015 JUL 31		2.49 10^8
	2015 AUG 01 2015 DEC 31		3.83 10^9
	2016 JAN 01 2016 JUL 17		0
Ash	2014 AUG 01 2014 DEC 31	1.6 10^7	0
	2015 JAN 01 2015 JUL 31		2.39 10^8
	2015 AUG 01 2015 DEC 31		3.18 10^9
	2016 JAN 01 2016 JUL 31		0
Nut	2014 AUG 01 2014 DEC 31	1.7 10^7	5.04 10^8
	2015 JAN 01 2015 JUL 31		0
	2015 AUG 01 2015 DEC 31		0
	2016 JAN 01 2016 JUL 17		2.16 10^8
Hatmehit	2014 AUG 01 2014 DEC 31	4.6 10^7	0
	2015 JAN 01 2015 JUL 31		4.97 10^8
	2015 AUG 01 2015 DEC 31		1.54 10^{11}
	2016 JAN 01 2016 JUL 31		0
Hator	2014 AUG 01 2014 DEC 31	1.81 10^8	0
	2015 JAN 01 2015 JUL 31		2.55 10^9
	2015 AUG 01 2015 DEC 31		3.39 10^{10}
	2016 JAN 01 2016 JUL 31		0

Table 4.3: Average values of absorbed heat Q_{abs}

Region	Area [m^2]	I [Wh/m^2]	Power-law index	Boulders size-range [m]
Seth/Ash	4.96 10^8	2.47 10^{14}	-4.2	7-30
Imhotep	1.9 10^7	4.91 10^{13}	-3.6	7-25
Khepry/Ash	2.9 10^7	2.36 10^{14}	-3.8	8-25
Ash	1.6 10^7	3.17 10^{14}	-6.4	7-30
Nut	1.7 10^7	1.83 10^{14}	-3.9	8-20
Hatmehit	4.6 10^7	2.47 10^{14}	-3.4	7-30
Hator	1.81 10^8	3.20 10^{14}	-5.2	7-40

Table 4.4: Irradiation values compared with power-law index and size-range of boulders.

4.3 Discussion

The investigated boulder distributions and irradiation model in this analysis generally revealed a trend in which to a greater degree of fracturing it corresponds a greater amount of solar radiation. On the comet nuclei, a larger fraction of the insolated energy is used for sublimation processes as consequence of a fast increase of temperature. In our analysis, we considered the surface of 67P as a collection of plate finite elements, in order to focus our attention on direct insolation effects, taking into account the inclination and position of a single region to the Sun. The general thermal balance equation of a single facet i is

$$Q_{abs,i} + \Sigma_j Q_{rad,ij} + Q_{con,im} + Q_{con,in} + Q_{sub,i} = Q_{cap,i} \tag{4.14}$$

and $Q_{abs,i}$ is the single major source term of the heat balance of a cometary nucleus. This absorbed heat quantity, and in particular its integral throughout the orbital period, is mainly responsible for thermal stresses on comet surface and resulting fractures or boulder formations. This is the reason why we focused just on this heat contribute, without considering for the moment the other terms, such as the radiative heat flux. Anyway, the self-heating between two surfaces or two surface elements i and j is

$$Q_{rad,i,j} = \varepsilon_i \varepsilon_j \sigma F_{ij} A_i (T_i^4 - T_j^4) \tag{4.15}$$

where σ is the Stephan-Boltzmann constant, ε is the IR emissivity facets i and j, and T is the absolute temperature of single facets. $F_{i,j}$ is the view factor between face i and j that are in radiative contact

$$F_{ij} = A_j cos\theta_i cos\theta_j / \pi d_{ij}^2 \tag{4.16}$$

which is valid in case of high emissivities $\varepsilon \simeq 1$ and $\mathrm{d}_{ij}^2 \geq A_i + A_j$, with d_{ij} distance between facets i and j. Θ_i and Θ_j are the angles between the surface element normal and the connecting vector between both surfaces. The ability of the surface to emit thermal radiation is expressed with this geometrical view factor Fij and it is very small for big spaces, but larger towards fracture or boulder components. The self-heating prevents from cooling down fast and looking to a similar analysis for fractures made by Hofner et al. (2015), unless the heliocentric distance is higher than 3.0-2.0 AU, self-heating does not significantly (less up 10%) add up to the energy budget if the surface is considered as a plate floor. Instead, at a distance of 1.25 AU, corresponding perihelion, the influence of self-heating is rising up to 45% of the solar irradiation. This leads one to think that the self-heating mechanism analyzed for fractures, which are another result of the same fracturing processes, is similar to what happens for boulder formation. What we therefore expect in future works is an increase irradiation of a quantity similar to the analyzed for fractures, equal to about 50% more at small distances from the Sun. We focused on the energy absorbed by cometary surface after the direct insolation, used to sublimate volatiles, because the resulting thermal stresses can fracture the surface, producing fractures and boulders. Analyzing the size-frequency distribution of boulders with diameters $\geq$ 7m, for slopes less 20° there is a large presence of boulders, isolated, far from high slope terrains and too large to be lifted by gas drag. For slopes steeper than 20°, there are terrains covered by dust and could be ancient boulder fields affected by degradation process of boulders and cliffs. In some regions, the boulder fields end on slopes lower than 20° and they could be the result of progressing eroding process of nucleus.
The assumptions at the basis of this thesis are that the comet, with a density equal to 0.4 g/cm^3, is made by a homogeneous material. Then, because of orbit inclination (7.04°), obliquity (52°) and spin axis with a right ascension of 69° and declination of 64°, the northern hemisphere is less illuminated that the southern, the neck less than the southern and the asymmetry of seasonal and diurnal insolation influences the shape and the morphology of the comet. More irradiation means more sublimation of ices and an increasing number of small boulders than those of a larger dimensions. The maximum solar flux on comet head is reached at heliocentric distance of 2 AU, instead the big lobe is fully illuminated during the perihelion passage at 1.2 AU. It also takes into account all models consider the 67P comet as a porous mixture of ices and dust, and with a very low tensile strength of the comet material. Another parameter useful to classify a region is the thermal inertia, a property

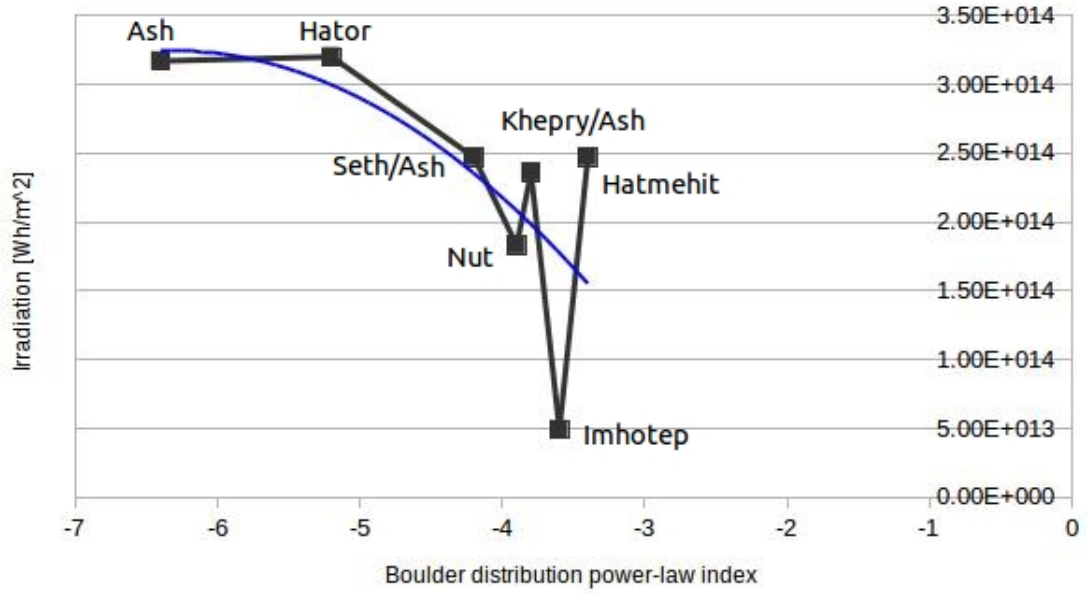

Figure 4.3: Correlation between boulders size-frequency distribution power-law index and irradiation in Wh/m^2.

related to thermal conductivity and volumetric heat capacity

$$I = \sqrt{\rho \lambda c} \tag{4.17}$$

with ρ the density of the comet, λ the thermal conductivity, and c the thermal capacity. A rougher consolidated material is characterized by I>50 J m^{-2} K^{-1} $s^{-1/2}$, a dust layer area has 10<I<25 J m^{-2} K^{-1} $s^{-1/2}$.
The compute of irradiation, i.e. the total amount of absorbed solar energy from the regions involved, has lead to table 4.4, in which each values of I, measured in Wh/m^2, are compared with the associated power-law index. These results are plotted in figure 4.3.

As it can see, the data trend respects the assumption that to a greater fracturing corresponds a greater amount of irradiation, and then the absorbed heat. From Ash to Imhotep things work well, although Khepry/Ash area differs a bit from the trend because of the greater area under consideration, being the irradiation proportional to the area. We find a strongly anomalous behavior of Hatmehit region, which has a low index and thus a low degree of fracturing, but a high irradiation value. Looking at figure 4.4, it is evident a more linear trend of the data, without considering the Hatmehit region. This anomaly reflects the one found in the article of Pajola et al. (2015) for the size-frequency distribution [29]: in fact, what they observe is a

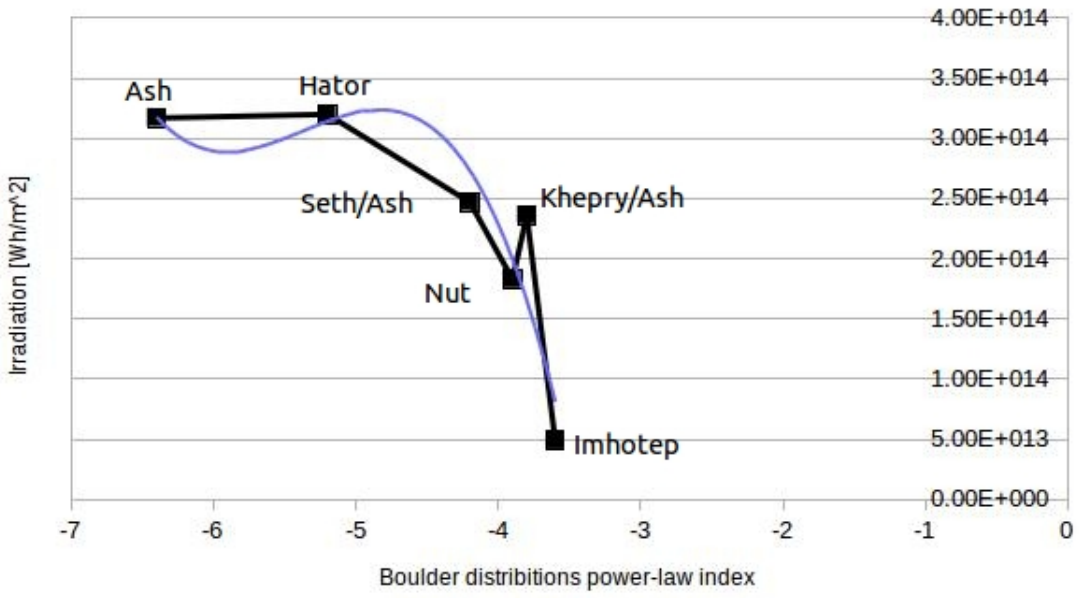

Figure 4.4: Correlation between boulders size-frequency distribution power-law index and irradiation in Wh/m^2, without considering the Hatmehit region.

slope distribution equal to -3.4, but in some areas this index reaches -1.0. In general, regions with high power-law indices of about 5 to 6.5 are high fractured and these areas have collapses and pits for- mation. Indices of 3.4 and 4 are markers for gravitational events due to sublimation of thermal stresses. Finally materials formed during gravi- tational phenomena or collapsing are characterized by a power-law indices of 1 and 2.
They suppose that the difference between the Hatmehit sub-regions can be interpreted as two different types of deposits, that is, different composition of the comet surface. In fact, the boulder size-frequency distribution in Hatmehit region shows a flex described by a power-law index equal to -1 or -2: this means probably that this boulders are mado of CO_2 and H_2O. Depending on the concentration of the two elements, the solar energy is sufficient to sublimate or less efficiently: the CO_2 ice sublimates at a temperature and pressure lower than H_2O ice, and for this reason, depending on the composition of the surface, we will have different products of fragmentation in size.

To support this hypothesis, two maps were compared: one contains the regions of the comet, centered on Hatmehit region, the other represents the distribution of CO_2/H_2O ratio in the same regions taken by ROSINA RTOF

mass spectrometer. The center of this map is the small lobe of the comet. ROSINA is a Rosetta Orbiter Spectrometer for Ion and Neutral Analysis, which includes two mass spectrometers to analyse the composition of neutrals and ions: RTOF, the Reflectron-type Time-Of-Flight (RTOF) mass spectrometer and the Double Focusing Mass Spectrometer (DFMS). As shown in figure 4.5, the water vapour mostly is found in the northern summer hemisphere near the neck region with cyclic diurnal variations whereas CO_2 was confined more to the southern hemisphere with a more spatially homogeneous composition [15].
Nut, Ash and Seth regions have a CO_2/H_2O=0/0.2, then there is a very low concentration of CO_2 ices. Imhotep and Khepry have a greater amount, from 0.6 to 1.0. For Hatmehit, as show in the red circle of the map 4.5, is very difficult to find an average value. There is a very wide differentiation of materials and ices in this region.

This important result shows and confirms that Hatmehit is a fundamental region that must be studied carefully: it is a border area between the northern rich water hemisphere and the southern hemisphere in which the CO_2 is predominant on the H_2O. The distribution of boulders presents high variability, consequence of the fact that this region is a mixed area in the composition, in which the fragmentation processes have a specific dynamic depending on the material in which they develop.

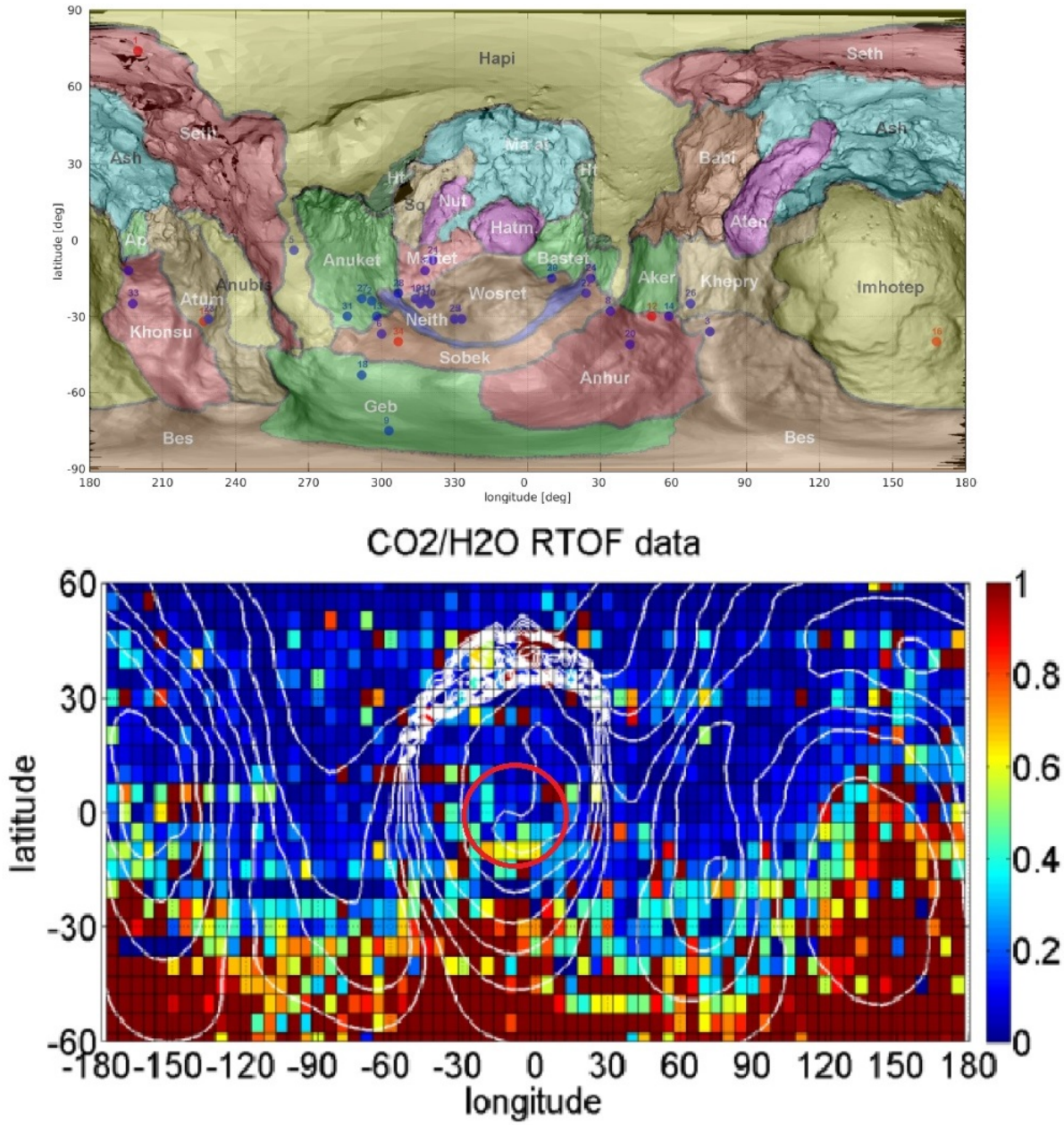

Figure 4.5: CO2/H2O detection maps from RTOF data recorded from mid-november 2014 until mid-february 2015. White line represents topography.

Conclusions

Comets, cosmic snowballs of frozen gases, rock and dust, are one of the most fascinating and changing object of our Solar System. These objects are so important because they represent the primordial part of our evolution, traveling almost undisturbed from the time of their formation. Furthermore, comets may not be able to support life themselves, but they may have brought water and organic compounds through collisions with Earth and other bodies of Solar System. Being object yet to be discovered, the European Space Agency designed the first mission capable of orbit around a comet, following it along its orbit, and land on it in order to obtain measurements in situ. This is the Rosetta mission, launched in 2004, whose objective was to achieve the short-period 67P/Churyumov-Gerasimenko comet. The spacecraft arrived at comet 67P in August 2014, entering the rendezvous phase. Rosetta and the Philae lander are equipped with several remote sensing and in situ instruments, able to study the physical and chemical properties of the nucleus, the evolution of the coma and of the nucleus during its orbit around the Sun, all of the morphological features present on the comet surface, and to analyze the development of the several regions interacting with the solar influence. In particular, the nucleus, its activity and the surface morphology of the comet has been observed by OSIRIS, the Optical, Spectroscopic and Infrared Remote Imaging System onboard Rosetta spacecraft. It consists of a high resolution narrow- and wide-angle cameras (NAC and WAC), able to resolve the nucleus up to 18.6 cm/px during the 10 km orbits around 67P. The images reveal that the comet 67P is characterized by two main lobes connected by a small neck. There is a clear dichotomy between the two lobes, and this appears in the form of contrasts on the comet surface: it can be observed smooth plains or highly fractured terrains, cliffs or pits, complex layers, fractures and boulder fields. All of these features derived from fragmentation processes that have affected, and still affect, the comet during its orbit. The fragmentation, i.e. the breaking of a continuous body into several pieces, depends on the physical regime in which the comet develop and it is controlled by energy argument. There are several causes at the ba-

sis of the fragmentation, such as thermal stresses, gravitational phenomena and comet activity, and the application of the fragmentation theory on 67P surface would allow us to understand the processes underlying the formation of fragments, such as fractures and boulders.

In this thesis we have started to understand the origin of the boulder deposits on the comet surface, analyzing one of the possible causes of the fragmentation, the irradiation on surface. The large obliquity (52°) and the orientation of the spin axis lead to a strong seasonal effects and to a thermal dichotomy: the northern hemisphere is relatively weakly illuminated, instead the southern is strongly insolated during the perihelion passage, at 1.2 AU. The absorbed heat flux of the comet surface is responsible for sublimation of water ices, but also CO and CO_2 ices, which sublimate at lower temperatures. This process fractures the surface, increasing the number of small boulders and eliminating smallest blocks containing water ice, reducing them into dust.

For these reasons, the first step of this thesis has been to compute the phase, the solar incidence and the emission angles during the orbit of the comet from 2014 August 01 to 2016 July 17. The choice of this time range has allowed us to analyze the irradiation amount and influence the year before and after the comet perihelion passage the 2015 August 13. This was possible thanks to and IDL code, in which were included the relative positions and the ephemerides of the bodies involved: the Sun, considered as the observer, the target, i.e. the comet 6P, and the spacecraft Rosetta. All of these data are available in an observation geometry information system for planetary science mission, the SPICE system, owned by NASA.
Once known the relative positions, were selected regions in which to analyze the presence of boulders, the same areas studied by Pajola et al. 2015 to find the size-frequency distribution power-law index of boulders with diameter larger than 7m. Ultimately we selected the following regions: Seth/Ash, Ash, Imhotep, Khepry/Ash, Nut, Hatmehit an Hator. The latitudes and the longitudes of these areas have been included in the code, in order to create a grid of points positioned on the shape file of the comet. Implementing the tassellated plate model, each of these areas is considered as a collection of single plate triangulars, and we did not consider the self-illumination between the different areas in order to focus firts on direct irradiation. The relative positions of these bodies were corrected for stellar and planetary aberrations, to obtain the apparent state of the target, its position and its velocity as seen by the observer, the Sun. At this point was possible to calculate the differents angles: the phase is the angle between the surface point-observer vector and the surface point-Sun vector, which in our case coincide.

We found only in part what we expected: following the analysis of the boulder size-frequency distributions, regions with high power-law indices of about -5 to -6.5 are high fractured and these areas have collapses and pits formation. Indices of -3.4 and -4 are markers for gravitational events due to sublimation of thermal stresses. Finally materials formed during gravitational phenomena or collapsing are characterized by a power-law indices of -1 and -2. Ash and Hator are strong fractured and as we expected the irradiance value is very high. Seth/Ash and Nut regions are characterized by fractured cliffs, niches an terraces and the specific power-law indices are due probably to gravitational processes and no activity or sublimation processes: the amount of irradiation decreases than before. Although Imhotep region follow the trend described above, something happened for this region and for Hatmehit in particular: they present a similar power-law index, but the amount of total absorbed heat energy is very different. Several causes can explain this different behavior, but in this thesis we support the hypothesis of a different percentage of ices, specifically the CO_2 to H_2O ratio, in the Hatmehit region, a border area between the northern hemisphere of the comet, rich in water, and the southern hemisphere in which the CO_2 is predominant. In this area, the fragmentation processes have a specific dynamic depending on the material in which they develop.

This variable strength and composition of surface material, coupled with the inclusion of self-irradiation in the future model, might be the key mechanisms working on the fragmentation processes.

4.4 Future projects

This is the knowledge we presently have about fragmentation and boulder formation on the 67P surface, but it is not sufficient to explain and connect all the previously described phenomena. This is the reason why we propose future research project, with the aim of making a fragmentation model that takes into account all of these, and possibly other, physical processes. In particular, the study of fragmentation on 67P surface could begin with a careful analysis of the thousands of extremely detailed images of the comet surface taken by NAC and WAC OSIRIS cameras. Thanks to the high resolution of this imaging system, and to the long period of orbiting around the comet also at a few km distance, it is possible to clearly observe from different perspectives a lot of complex layers, landslides, deposits, fractures and boulders which can provide plenty of useful information for this research. Specifically we propose to analyze all images containing boulders of different size and,

taking advantage of the already performed studies on the size-frequency distribution [29], all the regions where the boulders have already been cataloged. The different distributions need an explanation and for this reason the first step of the research will consist in analyzing the images discussed before, to characterize all regions containing boulders with their size-frequency distribution, and developing a database containing all the physical features of these objects. The basic assumption is that the boulders have to be originated by the same physical processes everywhere on the comet, and that their density is somehow related to the different fracture densities of the regions in which they are generated: thus, more fracturing would probably mean a larger number of boulders, as in the case of the head of the comet. After this classification, all studied regions must be connected with the relative comet surface temperature, because, as previously mentioned, one of the main processes responsible of the boulder fragmentation is definitely the thermal stress that the comet undergoes day by day during its orbit around the Sun. Thanks also to the data provided by VIRTIS, the Visible Infrared and Thermal Imaging Spectrometer on board Rosetta, it will be possible to create thermal maps by region and local illumination, also analyzing the temperature trend, knowing that the surface temperature depends on the physical properties of the surface, such as sublimation activity, bolometric albedo and emissivity. After that, the insolation and sublimation model, integrated along the 67P orbit, will be included to account for the different radiative energy amount that impinges on the different regions. The second part of the research will consist of including the gravitational phenomena and the cometary activity in the preliminary thermal fragmentation model: it will be necessary to analyze all OSIRIS images containing both geological features, such as scarps, deposits and fractures, and products of nucleus activity. We should identify the causes of formation of these features, studying the comet from a dynamic point of view, to include in the model the centrifugal and drag forces induced by the outflowing gas. This geological analysis will be done considering that the origin of terrains and morphological features are linked with the gravitational slopes, the nature of the cometary material and its mechanical properties, in particular tensile, shear and compressive strength.

The success of this project research will contribute to the knowledge on the formation and evolution of this magnificent object, fundamental for better understanding our Solar System origins.

Bibliography

[1] Bashkirov, A.-G. & Vityazev, A.-V. Statistical mechanics of fragmentation processes of ice and rock bodies. Planet. Space. Sci., vol.44, No.9, pp.909-915, 1996. PII: S0032-0633(96)00025-6.

[2] Beitz, E., Guttler, C., Jorda, L., et al. 2015, ApJ, 736,34.

[3] Capaccioni, F., Coradini, A., Filacchione, G. et al. 2015, Science, 347,628.

[4] Davidsson, B., Sierks, H., & G uttler, C. e. a. (submitted). The primordial nucleus of comet 67p/Churyumov-Gerasimenko. A&A,

[5] Duncan, M., Quinn, T., Tremaine, S., (1988). The origin of short-period comets. ApJ. DOI = 10.1086/185162,
adsurl = http://adsabs.harvard.edu/abs/1988ApJ...328L..69D,
adsnote = Provided by the SAO/NASA Astrophysics Data System.

[6] El-Maarry, M.-R., Thomas, N., Giacomini, L., et al. 2015. Regional surface morphology of comet 67P/Churyumov-Gerasimenko from Rosetta/OSIRIS images. A&A 583, A26. DOI: 10.1051/0004-6361/201525723.

[7] El-Maarry, M. R., Thomas, N., Gracia-Berna', et al. 2015. Fractures on comet 67P/Churyumov-Gerasimenko observed by Rosetta/OSIRIS. Geophys. Res. Lett., 42 , 51705178. DOI:10.1002/2015GL064500.

[8] ESA Rosetta blog (2015). URL: http://blogs.esa.int/rosetta.

[9] Fulle, M. 1997, A&A, 325, 1237.

[10] Gicquel, A., Vincent, J.-B., Agarwal, J. et al. (2016). Sublimation of icy aggregates in the coma of comet 67P/Churyumov-Gerasimenko detected with the OSIRIS cameras onboard Rosetta.

[11] Grady, D. Fragmentation of rings and shells. The legacy of N.M. Mott. Springer. ISBN:103-540-27144-9.

[12] Greenberg, J.-M. Making a comet nucleus. A&A, 330, 375380 (1998) adsurl = http://adsabs.harvard.edu/abs/1998A 26A...330..375G.

[13] Groussin, O., Jorda, L., Auger, A.-T., et al. 2015. Gravitational slopes, geomorphology, and material strengths of the nucleus of comet 67P/Churyumov-Gerasimenko from OSIRIS observations. A&A 583, A32. DOI: 10.1051/0004-6361/201526379.

[14] Gulkis, S., Allen, M., von Allmen, P., et al. 2015. Subsurface properties and early activity of comet 67P/Churyumov-Gerasimenko. Science 23 Jan 2015: Vol. 347, Issue 6220, DOI: 10.1126/science.aaa0709.

[15] Hoang, M., Garnier, P., Lasue, J., et al. (2016). 47th Lunar and Planetary Science Conference. The heterogeneity of the coma of 67P: ROSINA RTOF measurements and comparison with COPS and DFMS.

[16] Hofner, S., Vincent, J. -B., Blum, J., et al. 2016. The termophysics of fractures on comet 67P/Churyumov-Gerasimenko. A&A manuscript no. "Hoefner-Termophysics of fractures on 67P-draft 2016-04-04".

[17] Ian-Lin Lai, Wing-Huen Ip, Cheng-Chin Su, et al. (2016). Gas outflow and dust transport of comet 67P/Churyumov-Gerasimenko.

[18] Keller, H., Mottola, S., Davidsson, B., et al. 2015. Insolation, erosion, and morphology of comet 67P/Churyumov-Gerasimenko. A&A 583, A34. DOI: 10.1051/0004-6363/201525964.

[19] Keller, H. U., Barbieri, C., Lamy, P., et al. (2007). OSIRIS The Scientific Camera System Onboard Rosetta. Space Sci. Rev., 128 , 433506. DOI:10.1007/s11214-006-9128-4.

[20] Levison, H. F., & Duncan, M. J. (1994). The long-term dynamical behavior of short-period comets. Icarus, 108 , 1836. DOI:10.1006/icar.1994.1039.

[21] Levy Sara. Exploring the Physics behind Dynamic Fragmentation through Parallel Simulations. THSE No. 4898 (2010). ECOLE POLYTECHNIQUE FDRALE DE LAUSANNE.

[22] Lin, Z.-Y., Ip, W.-H., Lai, I.-L., et al. (2015). Morphology and dynamics of the jets of comet 67P/Churyumov-Gerasimenko: early-phase development.

[23] Lucchetti, A. SIMULATION OF EUROPAS WATER PLUME AND STRUCTURES RELATED TO ENERGETIC ACTIVITIES ON SOLAR SYSTEM BODIES FROM SATELLITE IMAGES. Ph.D School in Space Sciences, Technologies and Measurements Sciences and Technologies for Aeronautics and Satellite Applications.

[24] Martins Z, Price MC, Goldman N, Sephton MA, Burchell MJet al., 2013, Shock synthesis of amino acids from impacting cometary and icy planet surface analogues, NATURE GEOSCIENCE, Vol: 6, Pages: 1045-1049, ISSN: 1752-0894.

[25] Massironi, M., Simioni, E., Marzari, F., et al. (2015). Two independent and primitive envelopes of the bilobate nucleus of comet 67P. Nature, 526 , 402405. DOI:10.1038/nature15511.

[26] Migliorini, A., Piccioni, G., Capaccioni, F., et al. 2016. Water and carbon dioxide distribution in the 67P/Churyumov-Gerasimenko coma from VIRTIS-M infrared observations. A&A 589, A45. DOI: 10.1051/0004-6361/201527661.

[27] Mott, N.-F., Linfoot, E.-H. A theory of fragmentation. Ministry of Supply, A.C. (1943), p. 3348.

[28] Navigation and Ancillary Information Facility (NAIF) - NASA. http://naif.jpl.nasa.gov/naif.

[29] Pajola, M., Vincent, J. -B., Guttler, C., et al. 2015. Size-frequency distribution of boulders $\geq$ 7 m on comet

[30] Petrovic, J.-J. Review Mechanical properties of ice and snow. Journal of Materials Science (2003) 38: 1. DOI:10.1023/A:1021134128038.

[31] Pommerol, A., Thomas, N., El-Maarry, M., et al. (2015). OSIRIS observations of meter-sized exposures of H 2 O ice at the surface of 67P/Churyumov-Gerasimenko and interpretation using laboratory experiments. A&A, 583 , A25. DOI:10.1051/0004-6361/201525977.

[32] Preusker, F., Scholten, F., Matz, K.-D., et al. (2015). Shape model, reference system definition, and cartographic mapping standards for comet 67p/churyumov-gerasimenko stereo-photogrammetric analysis of rosetta/osiris image data. A&A, 583 , A33. URL: http: //dx.doi.org/10.1051/0004-6361/201526349. DOI:10.1051/0004-6361/201526349.

[33] Rickman, H., Marchi, S., A'Hearn, M.-F., et al. 2015. Comet 67P/Churyumov-Gerasimenko: constraints on its origin from OSIRIS observations. A&A 583, A44. DOI: 10.1051/0004-6361/201526093.

[34] Sierks, H., Barbieri, C., Lamy, P. L., et al. (2015). On the nucleus structure and activity of comet 67p/churyumov-gerasimenko. Science, 347 . URL: http://www. sciencemag.org/content/347/6220/aaa1044.abstract. DOI:10.1126/science.aaa1044. arXiv:http://www.sciencemag.org/content/347/6220/aaa1044.full.pdf.

[35] Singh, M. & Singh, B. Rock Mech. Rock Engng. (2005) 38: 243. A Strength Criterion Based on Critical State Mechanics for Intact Rocks. DOI:10.1007/s00603-004-0042-3.

[36] Thomas, N., Sierks, H., Barbieri, C., et al. 2015b, Science, 347,440. 67P/Churyumov-Gerasimenko. A&A 583, A37. DOI: 10.1051/0004-6361/201525975

[37] Thomas, N., Sierks, H., Barbieri, C., et al. (2015). The morpholog- ical diversity of comet 67p/churyumov-gerasimenko. Science, 347 . URL: http://www.sciencemag.org/content/347/6220/aaa0440.abstract. DOI:10.1126/science.aaa0440. arXiv:http://www.sciencemag.org/content/347/6220/aaa0440.full.pdf

[38] Tosi, F., Capria, M. T., Capaccioni, F., et al. (2015). Thermal maps and properties of comet 67P as derived from Rosetta/Virtis data. 46th Lunar and Planetary Science Conference.

[39] Vincent, J.-B., AHearn, F., Lin, Z.-Y., et al. 2016. Summer fireworks on comet 67P.